UNIVERSITY OF SOUTHAMPTON

SPECTROSCOPIC STUDIES OF SUBSTRATES USED FOR SOLID-PHASE
SYNTHESIS AND COMBINATORIAL CHEMISTRY: FUNDAMENTALS AND
APPLICATIONS

By Abigail Rose

Thesis submitted for the Degree of Master of Philosophy

October 2000

UNIVERSITY OF SOUTHAMPTON

ABSTRACT

FACULTY OF SCIENCE
CHEMISTRY

Master of Philosophy

SPECTROSCOPIC STUDIES OF SUBSTRATES USED FOR SOLID-PHASE
SYNTHESIS AND COMBINATORIAL CHEMISTRY: FUNDAMENTALS
AND APPLICATIONS

by Abigail Rose

Combinatorial Chemistry has become an extremely efficient method of producing
chemical compounds in the last twenty years, but the resin beads that are used in
this method of solid phase chemistry are little understood. The work presented in
this thesis is concerned with using scanning confocal Raman spectroscopy to
investigate the properties of the polymer beads and the distribution and properties
of cyanobenzoic acid once loaded onto the support. The beads act as a lens, the
AFM results show that the surface is smooth above 0.1 μm.

It was found that the cyanobenzamide tag is approximately evenly distributed in
the bead. The tag is distributed in all areas where there is polymer. Mapping the
whole area of a dry bead showed that areas of higher concentration of tag were
found in very small-localised areas. Swollen beads showed a very even
distribution of tag. The tag was found to have a slightly non-linear relationship
between loading and peak intensity. This was attributed to the change in
environment as the molecules came closer together and the intermolecular
interactions between them. These interactions produced a shift to higher
wavenumbers with higher loading of the nitrile stretch.

The intensity of the Raman peak as a function of distance down through the
bead (z-direction) is seen to be symmetric about the bead centre for the
swollen beads but a distinct asymmetry is observed for dry beads.. This is due to
the refraction of light at the air/bead interface leading to the bead acting as a lens.
A discrepancy is observed in the size of the dry bead in the z-direction and x-y
plane this is equal to the ratio of refractive indices of air and polystyrene.

Acknowledgements

I would like to thank the many people who have helped me over the past year. Firstly I would like to thank my supervisor Dr Jeremy Frey for all his support and ideas over the last year. I would also like to thank Dr Bill Brocklesby and Prof. Mark Bradley for their scientific knowledge and help during brainstorming sessions. Without Dr. Andrea Russell I would not have been here this year, so I thank her for giving me the opportunity to do my MPhil.

This year would not have been the same without the collaboration with Dr. Jürgen Kress and our sitting in a dark room waiting for a peak! Thanks for making this year enjoyable and for making the beads, because without them there would be no MPhil.

Thanks must also go to Renishaw for all their expert help with the instrument and for answering the endless stream of email enquiries.

I would also like to thank the Russell Group for all their help and for keeping me sane over the last year.

TABLE OF CONTENTS

1   INTRODUCTION

## 1.1   Combinatorial Chemistry

1.1.1   Overview

Combinatorial Chemistry has developed in the last twenty years into an extremely efficient way of generating molecules to be used in drug discovery[1-3]. It was a novel technique when it was developed, as combinatorial chemistry uses solid phase substrates for synthesis whereas traditional chemistry is performed in the liquid phase. The essence of combinatorial chemistry is that many compounds can be synthesised simultaneously. This is done in a parallel manner, in traditional chemistry one compound is generated for every step in the synthesis, in multi-parallel synthesis many compounds can be produced for each step. One of the first ways was the use of 'T-bags' as porous containers containing solid phase beads, the same peptide coupling step was performed on each bag irrespective of what sequence was already attached to the bead. In the late 1980's Furka described the mix and split procedure. Equal portions of the solid support are divided into portions and reacted with different monomeric starting material. The coupling reaction is then pushed to completion by using excess monomer reagent and then washed to remove the excess. The individual portions are then mixed, redistributed into portions again and reacted with a further set of reagents. This whole process is then repeated as necessary (for a total of n times), the number of compounds generated is described by the below equation

No. of Compounds $= x^{n}$ **Equation 1.1**

where x is the number of different monomers. Therefore for a 3-monomer system with three reactions twenty-seven compounds would be generated (3^3). This range of compounds is described as a library, as the compounds are all related. The compounds can be in the form of a linear library or a template library.
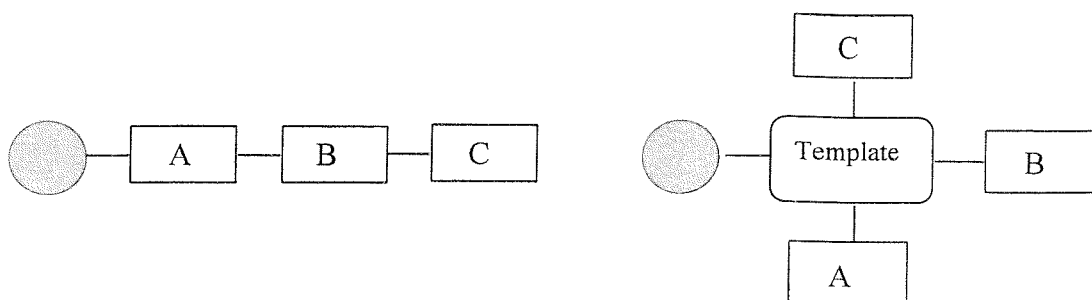
Figure 1.1   **Example of linear and template libraries. A, B, C can be the same monomer unit or different.**

The preferred solid support is polymer beads but grafted polymeric pins, paper or polymer sheets and even glass chips have been used to immobilise the reacting compounds.

1.1.2   Advantages of Solid Phase Chemistry

The use of solid phase chemistry has many advantages over liquid phase synthesis. When used industrially the process can be automated by the use of robotics, which can handle 96 samples at once when arranged in arrays. The 96 (12 x 8) well plates are used traditionally but due to automation these plates can be continuously handled by the robotics, therefore an enormous number of samples can be prepared very easily. By the use of mass action, high concentrations of reagents can be utilised. As rate is proportional to concentration the rates of reaction are much higher in solid phase chemistry. In excess of a 99 % yield is possible due to repetition of the chemistry until the desired yield is obtained. In solution phase chemistry:

$$A + B \rightarrow C$$

An excess of A would not be added to drive the reaction whereas in solid phase chemistry:
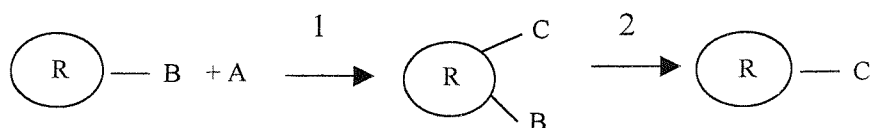
Figure 1.2   **A typical solid-phase reaction.**

After step 1 (Figure 1.2) the beads are washed to remove A, step 2 is then repeated until just the product (C) is attached to the resin. Purification is then performed in a similar way. Most reactions in combinatorial chemistry are performed in mini-plastic syringes with a filter on the bottom, this way the washing step is extremely simple and can also be automated. For effective washing the solid phase is washed many times in alternating polarities of solvent, for example, a polystyrene resin would be washed in dioxane to swell the bead to rinse out impurities and then water which would shrink the resin. This process is then repeated about 12 times to ensure the beads only have the product left attached to them.

1.1.3 Disadvantages of Solid Phase Synthesis

One of the main disadvantages of solid phase synthesis is that reaction analysis is not possible in the traditional way. Reaction analysis is important as it can profile a reaction, be used for quality control in libraries and help with lead generation.

In solution phase chemistry Thin Layer Chromatography (TLC) is used as a routine tool to determine whether a reaction has gone to completion. With the products attached to the resin in solid phase synthesis this is not possible. Nuclear Magnetic Resonance (NMR) is also more problematic, to achieve a normal NMR the product needs to be cleaved from the resin. C-13 Gel Phase NMR can be performed with the compound attached to swollen resin, but this produces broad linewidths due to a lack of molecular mobility. Another problem is reaction optimisation, with such a wide range of monomers in combinatorial chemistry it is harder to ensure that all reactions proceed as efficiently as they can. (see section 1.2.3 for more detail)

1.1.4 Solid Phase Supports

As explained earlier there are a many different supports that can be used in combinatorial chemistry. This report will only describe polymer beads, as these have been the focus of this work. There are several types of polymer bead commonly used, the most common being polystyrene resin. It is very cheap and easily made by stirring styrene with di-vinylbenzene (DVB) in suspension with

3

water. The bead size (20- 200 µm) is determined by the speed of the stirring, faster stirring produces smaller beads. Polystyrene beads are robust; the level of DVB (typically 1-2 %) governs this property. Less than 1 % will produce fragile beads and greater than 3 % will produce beads that do not swell effectively. The advantageous properties of polystyrene beads are their robustness as described above, they are also insoluble in all solvents. Polystyrene beads are chemically and physically stable and various bead sizes can be obtained which have loadings of 0.5 –5 mmol g^{-1}. Polystyrene beads readily solvate and swell to five times their dry volume. One of the drawbacks of polystyrene resin though is its hydrophobic nature. This can cause problems in peptide synthesis, as both the peptide and resins are not equally expanded in the reaction conditions and the rate and yield are adversely affected. These problems resulted in the development of polar solvent compatible resins such as TentaGel.

TentaGel is a polystyrene resin with tentacles of PEG (PolyEthylene Glycol) attached through an ether link. It is this added functionality that makes TentaGel much more mobile than polystyrene, as when solvated the PEG groups are free moving and in a solution-like environment. The polyethylene glycol chains make up about 75 % by mass of the beads. The polystyrene framework of TentaGel provides a non-constricting support, which retains open channels for diffusion of reagents and solvents through the resin. One disadvantage of this solid support is its loading density of about 0.25 mmol g^{-1}, compared with 0.5-1.2 mmol g^{-1} of polystyrene.

1.2 Reaction Analysis in Combinatorial Chemistry

The main use of reaction analysis in combinatorial chemistry is the deconvolution of libraries. In the example illustrated previously (page 1) a small library (27 compounds) was formed but libraries up to the size of one million compounds can be made easily in a few days. The problem then is to discover what is on each bead and if it is pharmacology relevant (for example). Each bead can only have one compound on it, and there are two main ways to track or discover what it is. One way is tagging, on each step a tag is added at the same time as the reaction is

carried out. The other method is using spectroscopic methods to discover the compound on the bead. I will therefore discuss these two methods separately.

1.2.1 Tagging

The basic principle for encoding is that every bead within the library has synthesised upon it a tagging compound that encodes uniquely for the library compound on the bead. The coding tags reveal the synthetic history of the bead. The tag needs to be easily interpreted using spectroscopic or other analysis techniques sensitive to the small amounts present. Libraries prepared through the mix and split method benefit most from tagging strategies.[4,5]

There are several requirements that a tag must satisfy to be effective.[4]:

- The tag must be synthesised in parallel to the synthesis of the library molecule; therefore the reaction chemistry for both must be compatible.
- The tag must be physically separable from the library compound and should be interpreted without interference from the library component. Ideally the library component should be removable by mild cleavage but the tag should be left behind for either on-bead analysis or analysis after more vigorous cleavage.
- The tag must be present in very low concentrations so that library components can be attached in large loadings to the bead.
- The tag must be easily sequenced otherwise the encoding scheme does not offer any advantage over the structural analysis. The most recent tagging schemes generate a mixture of encoding molecules that can be read via a chromatographic separation as a binary code that directly reveals the synthetic history of the bead

Tags can be easily divided into two main types, chemical and non-chemical so I will briefly discuss these two different methods. The first chemical tags to be developed were peptides and oligonucleotides but they had many disadvantages so one of the newer types of tags is a haloaromatic tag, which are chemically inert. With this type of encoding there is not one for one correlation between the library monomer and encoding molecules. It is the presence or absence of a limited set of tagging molecules, which are detected by electron capture capillary electrophoresis.

Capillary electrophoresis can rapidly and efficiently separate tiny quantities of material, which is why it is particularly suitable for the analysis of tags.

Molecular encoding can produce problems due to the incompatibility of the tagging chemistry and the synthesis chemistry of the library component. Therefore non-chemical tags have been developed such as radio frequency tags which when placed in a porous inert container of resin beads the chip can be tracked by its individual code.

Encoding by fluorophores has been investigated. Scott *et al* [6] found that fluorophore tagging was highly sensitive. The loading on the beads was less than 1 pmol/bead and similar properties were observed to the solution phase. At a low level the excitation and emission bands were not shifted and no self-quenching was observed. Different dyes can be used as tags as the deconvolution of peaks is easily done and fluorescence intensity can be quantified. Above 5 % loading self-quenching was observed but at lower loading a linear relationship was found between the amount of resin bound fluorophore and fluorescent intensity. Therefore an encoding strategy is proposed using different levels of dyes. Egner *et al* [7] proposed a similar technique and encoded a small library, the first residue corresponded to a different dye. The spectra of the dye were obtained by the use of fluorescent confocal microscopy; different dyes were used that all had unique emission and excitation spectra and could easily be identified. The advantages of fluorescent encoding are that deconvolution does not require cleavage of the library molecule or tag and the technique is non-destructive. The disadvantage is that the fluorophore tag may potentially have poor chemical and photochemical stability.
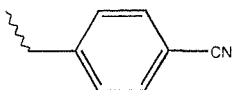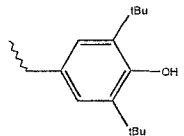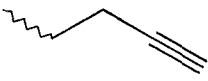
It has been shown that fluorophores have good potential for tags in split and mix library creation on the solid phase, but to fully understand their behaviour on the bead, the properties of the dyes in solution should be studied.

In solution it is well known that xanthene dyes form aggregates at high concentration, these aggregates are believed to be dimers, possibly trimers or higher aggregates. Both Rhodamine 6G and Rhodamine B in water have absorption spectra that consist of two peaks separated by about 25 nm, at lower

wavelength the peak is attributed to the dimer and at higher wavelength to the monomer, on changing the concentration spectra pass through an isobestic point. In ethanol however both xanthene dyes were found to follow beers law and dimers didn't form.

S. Rahman and co-workers [8] used Infrared and Raman spectra to analyse Sasrin beads encoded with either Raman and/or infrared active groups. The beads could be unambiguously identified from their Raman and FTIR spectra. They used functional groups with characteristic vibrational frequencies in the less crowded 4000-3500 cm^{-1} and 2800-1800 cm^{-1} regions. The tags were attached in different combinations. The spectra were collected from a 1 μm diameter area of a flattened bead.

Table 1.1   Frequency (cm^{-1}) of Infrared and Raman Tags [8]

Structure	Infrared Signal	Raman Signal
	2231	2230 - 2131
	3624	N/A
	2120	2119 - 2120

They conclude that FTIR and Raman microspectroscopy could be used to develop a novel encoding strategy for deconvolution of library hits and suggest that an encoding method would involve the co-synthesis of a set of Raman and IR active tags to label the synthetic sequence. Other groups that could be used as tags include:

-C≡C-D   2585-2630 cm^{-1}

-C=C-D   2225-2335 cm^{-1}

-C – D   2685-2255 cm^{-1}

-C=C-C≡N   2215-2240 cm^{-1}

-N=N=N   2120-2160 cm^{-1}

And specifically Raman tags

CH_2NO_2 1375-1390 cm^{-1}

$ArNO_2$ 1310-1355 cm^{-1}

C-S-S-C   505-515 cm^{-1}

(where Ar = Aromatic group)

An advantage of these tags is the ability to access the encoding information while the tags are still attached to the resin.[8]

1.2.2   Spectroscopic Methods of Library Deconvolution

On bead analysis is the most useful type of method as it saves time and money and can be automated. There are only a few methods at present, which are capable of providing quality data, these are described below.

One of the most simple of analysis techniques in combinatorial chemistry is the Ninhydrin test; this is a spectroscopic technique involving primary amines. In Aminomethylated polystyrene it is the amine functionality that attaches the monomers to the resin. The ninhydrin molecule attacks the unreacted groups and the resulting blue colour at 570 nm is measured by an uv-vis spectrometer. This process is then both qualitative and quantitative. When compared with an unloaded bead, the loading levels of the bead can be determined. Other colourmetric procedures are available which monitor thiols, hydroxyls, aldehydes and acids.

Gel Phase NMR with the resin swollen in solvent is possible, ^{13}C provides much better results than ^{1}H because of the broadening of the linewidths. This method is more qualitative than quantitative when used with resins due to the high signal to noise ratio of about 5 % and is therefore a good method for reaction monitoring.

Vibrational spectroscopy has been used for reaction analysis and real-time monitoring with infrared spectroscopy being the most widely used[9-14]. With a FT-IR microscope single bead analysis is possible, the bead is often flattened to give better signals. The drawback of this method in routine analysis is the cost of the equipment. A cheaper version is ATR (Attenuated Total Reflection) where single bead analysis is possible but more commonly several beads are analysed at once.

The ATR crystal flattens the beads and the ATR accessory will fit any standard IR instrument.

In his paper, Hans Gremlich [15], reviewed the use of optical spectroscopies in combinatorial chemistry. He describes how the many techniques are applicable to analysis of the solid supports used and the products attached to them. The various methods and the information obtained are summarised below.

With Infrared Transmission Spectroscopy, 1-3 mg of finely ground solid sample is prepared as a potassium bromide disc. Diagnostic bands can be identified and each reaction step can be monitored directly on the bead. This then provides qualitative analysis throughout the reactions. The disadvantage of this method is the large amount of resin needed and the fact that it is a destructive technique. Internal reflection spectroscopy (or Attenuated Total Reflectance, ATR) is a non-destructive form of IR. For combinatorial chemistry internal reflection spectroscopy can be applied to beads and many accessories have been designed for pins and crowns (another type of solid support used in combinatorial chemistry) which can make the analysis very straight forward and efficient.

Infrared microscopy permits samples in the picogram range to be analysed. It is a totally non-destructive method and requires no sample preparation as the reaction products can be monitored directly in a single resin bead without the need for cleavage. Infrared spectra of single beads have been used for real time monitoring of solid phase reactions.

Photoacoustic Spectroscopy is a fast non-destructive method for analysing various materials, which requires no sample preparation. The photoacoustic effect arises from the fact that infrared radiation absorbed by the sample is converted into heat within the sample, this heat diffuses to the surface and into an adjacent gas atmosphere. A microphone detects the photoacoustic signal. This method is less sensitive than ATR spectroscopy but offers a convenient alternative to infrared techniques.

Liquid Chromatography is a technique extensively used in separations in combinatorial chemistry; it can provide quantitative data when the identities of the mixture components are known. IR spectrometers have been interfaced to HPLC and IR spectra can be collected from spots of sample, which contain μg amounts by the use of special optics. HPLC-MS is already used extensively in combinatorial chemistry and HPLC-IR can provide a good compliment to it. TFA (Trifluoroacetic acid) is often used for cleaving the sample from the solid support but this can severely obscure a LC-IR spectrum so it must be removed prior to analysis. This can be overcome by using a LC-IR Transform™ which is a solvent elimination system, the IRC (Infrared Chromatograph) provides full FT-IR spectra of the eluent stream from a LC column. A pneumatic linear capillary nozzle is used to remove the mobile phase from the samples as they pass through a hot flowing sheath gas that evaporates the solvent. The sample is then deposited onto a Germanium sample collection disk as spots of sample, IR spectra are then taken of these dry spots.

Gremlich concludes that IR and Raman spectroscopy are advantageous due to the lack of sample preparation but there can be problems in monitoring reactions with no changes in functional groups.

1.2.3   Monitoring of Solid Phase Reactions

Bing Yan and co-workers [16] compared the application of FTIR and FT Raman in the reaction optimisation stage of combinatorial chemistry. They used FT-IR micro-spectroscopy, a beam condenser, ATR, macro and single bead FT Raman spectroscopy, KBr pellets, DRIFT and Photoacoustic spectroscopy. These various techniques were used to obtain spectra for ten different resins carrying diverse functional groups. A comparison was drawn between the different techniques in different categories such as spectral content and quality, sample requirements, speed and instrument cost. It was concluded that for a method to monitor solid phase organic reactions, single bead FT-IR provides the best analysis method in the shortest of time. They then went on to compare these methods for monitoring solid-phase organic reactions. The KBr pellet method was not used, as it was not

suitable for continuous analysis. FT Raman cannot detect hydroxyl stretching due to Raman selection rules so could not be used in this experiment and ATR was not used due to moisture interference in the hydroxyl stretching region. The reaction was monitored by the disappearance of starting material bands and the formation of bands attributable to the product. The integrated area of the emerging band was plotted against time and fitted to a pseudo first order rate equation with a rate constant of $3.8 \times 10^{-4} s^{-1}$. The main conclusions were that single bead and beam condenser FTIR methods could be used as a TLC equivalent for solid phase synthesis because only 50-100 beads are needed for analysis, so removal of the small amount does not disturb the reaction; high quality spectra can be recorded within minutes. Sample preparation is not required and the two FTIR methods provide qualitative and quantitative kinetic information on organic reactions carried out on solid supports.

D. Pivonka [17] looked at on-bead quantification of resin bound functional groups. The two methodologies used are designated 'analogue bleed' and 'dual analogue'. The target functionality through the experiments was the chloromethyl functionality of chloromethylstyrene.

In the 'analogue bleed' experiment an infrared microscope and infrared flow cell (which allowed an identical spectral path length) to analyse dry beads. The beads were measured dry and then different concentrations of benzyl chloride were bled into the cell and spectra collected. The analogue bleed analysis produced a $-CH_2Cl$ loading value very close to the value stated for the loading obtainable by the bead manufacturer.

The 'Dual Analogue' quantification method is based upon base resin to pendant functional group band ratios using solution phase analogue standards for both the resin and pendant group. Un-cross-linked polystyrene was added to known quantities of benzyl chloride. The mixtures were then dissolved in CCl_4 to provide homogeneous solutions. These solutions provided calibration against spectra of swollen candidate beads.

In the Raman experiment standard and swollen aminomethylstyrene beads were placed in separate NMR tubes for analysis. Regression analysis yielded a R^2 correlation of 0.996 but there were only 3 data points in the set. They conclude that quantification methods provide simple yet robust technology for quantification of a wide range of pendant functional groups throughout polystyrene-based solid phase synthesis.

1.3   Aim of the Project

As I have illustrated in the previous sections there has been a huge amount of research carried out into combinatorial chemistry in the last twenty years but mostly on the organic chemistry side. The use of vibrational spectroscopy in solid phase synthesis has not yet been fully explored.

The aim of this project is to use confocal Raman spectroscopy to investigate both the nature of the resin beads and the distribution and properties of tags once loaded onto the beads. There is only a very small section of the literature dedicated to the distribution of molecules once attached to the bead. Combinatorial chemists use beads daily in the synthesis of libraries but don't really know where their reaction occurs, whether it is on the surface of the bead, in the middle of the bead or both. There is then the question of the fine structure of the bead whether the formation of the bead leads to a homogeneous structure or if voids are formed.

As I have shown earlier when using fluorophores as tags the loading can affect the properties of the dyes. In this investigation we use cyanobenzoic acid as a tag to investigate the bead's distribution of sites, the use of a non-fluorescent compound overcomes some of the problems associated with fluorescent tags.

2   EXPERIMENTAL METHODS

2.1   Raman Spectroscopy

Raman spectroscopy was established as non-destructive analytical technique in the 1930's. The principle of the Raman process is that radiation incident on a sample is scattered inelastically.

When the laser light interacts with the molecules it can be scattered in two ways. Elastic (Rayleigh) scattering occurs when the oscillating electric field associated with the light interacts with a molecule. A small dipole moment is then induced through the polarisability of the molecule. This induced dipole oscillates at the same frequency as the laser (v_0). The oscillating dipole radiates light at the same frequency at which it oscillates. As this light is not radiated in the same direction as the exciting light, it is said to be scattered. The other type of scattering occurs because the molecules themselves are vibrating at frequencies, which correspond to different modes of motion. The vibrational frequencies mix with the exciting light to form sum and difference frequencies, ($v_0 + v_{vib}$), and ($v_0 - v_{vib}$) in the scattered light. This process is inelastic and named after C.V. Raman (Raman scattering). It is much weaker than Rayleigh scattering, typical intensity ratios for pure liquids are $\sim 10^3$. Light scattered at frequency ($v_0 + v_{vib}$) is known as Anti-stokes Raman scattering, light scattered at ($v_0 - v_{vib}$) is termed Stokes Raman scattering.[18] The following diagram shows the transitions involved.
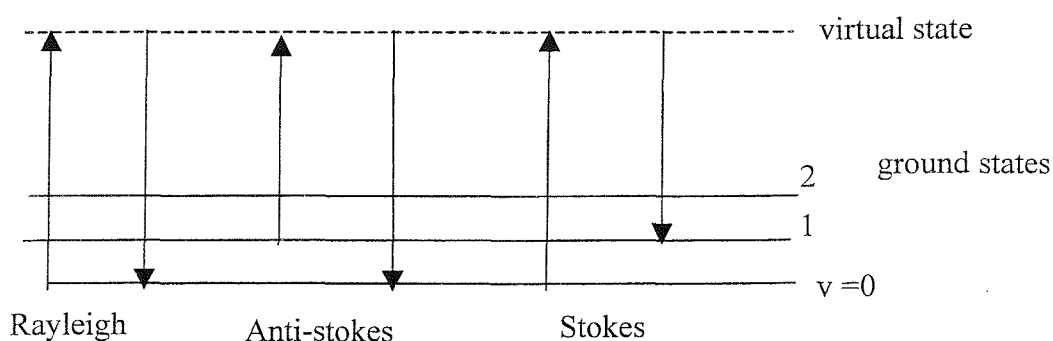

Figure 2.1   Diagram of Stokes, Anti-stokes and Rayleigh lines.

The relative intensities of the Stokes and anti-Stokes scatter are depend on the populations of the ground state and first excited vibrational state. These are given by the Boltzmann distribution.

$$\frac{n'}{n} = \frac{g'}{g}\exp\left(\frac{-\Delta E}{kT}\right)$$

Where n is the population, g is the degeneracy and ' denotes the upper level.

As seen in the below diagram the Stokes scatter is more intense and thus this side is scanned.
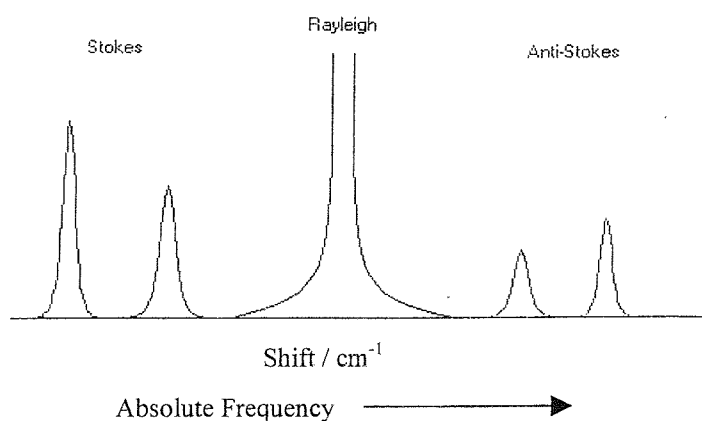

Figure 2.2   Plot of Anti-Stokes and Stokes Raman Bands

Raman scattered light can be produced from an excitation source with any wavelength of radiation and therefore Raman spectra are presented as intensity vs. frequency shift from this excitation source. The Raman scattering efficiency depends on the 4th power of the frequency of light being scattered, so the relative band intensities will differ depending on the excitation source used.[19]

The vibration of a bond changes the degree of orbital overlap and may change the molecular polarisability and the dipole moment of that molecule. A vibrational mode is Raman active if it possesses a change in polarisability (α), therefore only some modes are Raman active. If a bond has a change in dipole moment during a vibration it is infrared active. If a molecule has a centre of inversion, a rule of mutual exclusion applies; a vibration is then observed in either Raman or infrared but not both.

14

2.1.1 Renishaw 2000 System

The layout of the Renishaw imaging microscope is shown in the diagram below.
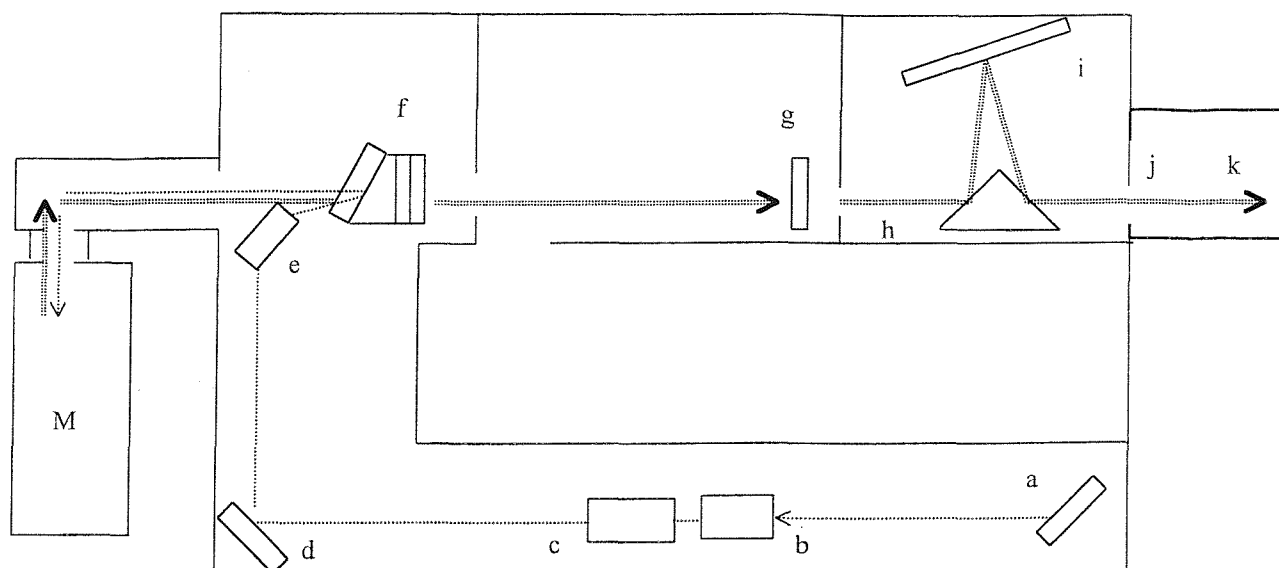
**Figure 2.3   Raman optical main assemblies.**

Key:

a	Laser alignment mirror.
b	x40 objective lens and 10 μm pinhole.
c	x4 objective.
d	Adjustable mirror.
e	Fixed mirror.
f	Holographic notch filter and polariser/ waveplate.
g	Spectrographic entrance slit assembly
h	Prism mirror
i	Diffraction grating assembly
j	CCD focusing lens
k	CCD detector
M	microscope
....	Laser light
═══════════	Raman light

The laser light is directed along a,b,c,d,e and f, the laser and Raman scattering is directed back through the microscope to f, Raman light only is then directed along. g,h,i,j,k, when in the grating mode. When a static scan is performed the grating (i) is held motionless during the experiment hence the experiment is called a static scan. An extended scan is used when the spectra need to have a larger range of wavenumbers, in the case of the extended scan the grating moves during the experiment. The advantage of the extended grating scan is that it improves the

signal to noise ratio as the scanning averages out the pixel to pixel differences as each spectral element is scanned across the whole of the CCD camera.

2.2 Confocal Microscopy

The Renishaw Raman imaging microscope used in these experiments has the ability to be used in confocal mode. Confocal microscopy allows information to be collected from a small well-defined optical section of the sample, rather than a larger section of the sample in conventional imaging. In both confocal and conventional imaging the collection volume is limited by the optical properties of the sample and the optical configuration of the instrument. The difference in confocal imaging is that these parameters can be adjusted to allow a very small volume to be imaged. When the instrument is set to the correct parameters for confocal microscopy it ensures that light that is in focus with the Raman system is accepted but light from the surrounding area which is out of focus is rejected. This is because the focus is very sharp due to the use of a very small aperture for both illumination and detection.
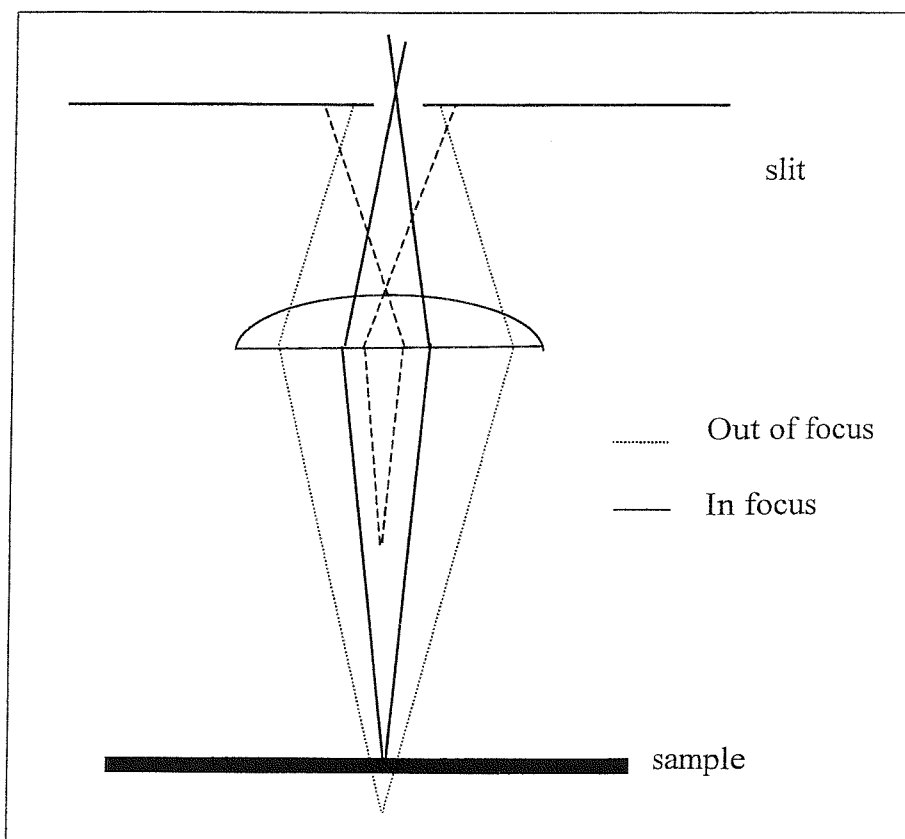
Figure 2.4   The basic principle of a confocal microscope.

As can be seen in Figure 2.4 the rays that are not in focus do not enter the detector and are not recorded.

The advantages of confocal microscopy are that true, three-dimensional data sets can be recorded. The sample can be scanned in the x/y direction as well as the z-direction and by image processing slices of the sample can be superimposed giving a three dimensional focus image at a typical resolution of about 1 μm x 1 μm x 3 μm (see
Figure 2.6).

The effect of setting the system to be confocal is to improve the spatial resolution, this means to improve the ability of the system to discriminate between closely spaced objects. In a conventional system pinholes are used to point-like illuminate and point-like observe. The illuminating light is focused through a lens then a small aperture, the light from this pinhole is then focused into the sample. The light emerging from the sample is collected in a similar way but in reverse, the light is directed through the pinhole and onto the detector. As the pinhole is so small this only allows in-focus light through, eliminating spectral features not associated with the area of interest.[20] In the Renishaw Raman system a pinhole is not used, but the slit and the capture area on the CCD array are altered to perform the same function. The slit (position g Figure 2.3 is closed down to a width of 10 μm which only allows light through of the right focus in the x direction, the CCD pixel height is then reduced which discriminates light in the y direction (see Figure 2.5). It is necessary to ensure the correct alignment of the beam, as this means that the maximum possible excitation energy is being concentrated into the area that is being analysed. In these experiments this alignment is carried out with a silicon wafer. The beam is focused onto the silicon and is centred with the crosshairs, the beam is then defocused to ensure that it diverges into concentric rings which are centred around the crosshairs, small adjustments are then made to mirrors d and e (see Figure 2.3).
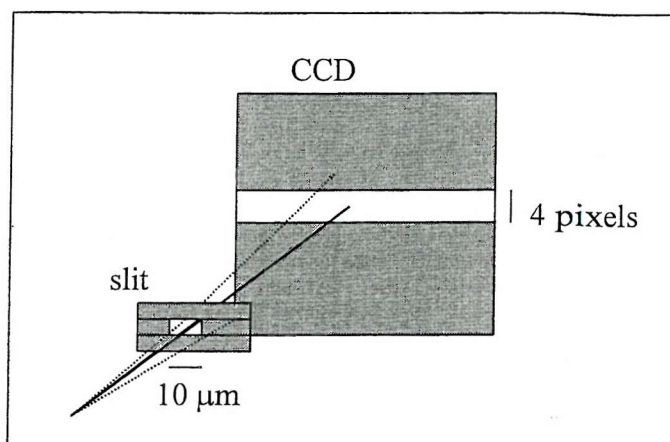
Figure 2.5 **Diagram to show the action of the slit and CCD array in the Renishaw 2000 system.**

The wavelength of light (λ_{exc}), the numerical aperture (NA) of the objective used and the diameter of the diaphragm determine the depth of the focal plane. These are related by equation 2.1[21]
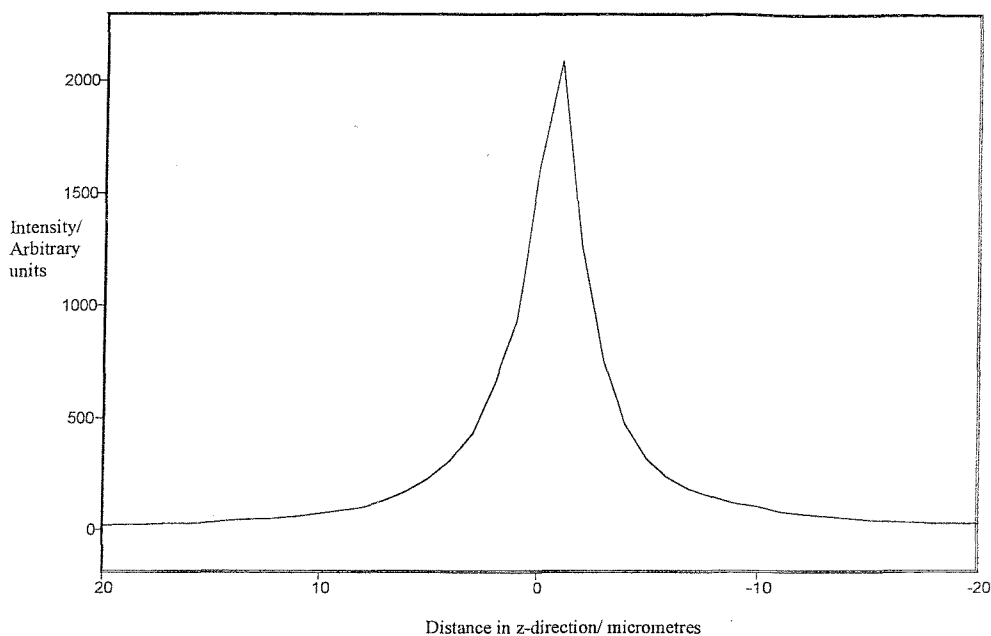
$$dz = \frac{0.64 \times \lambda_{exc}}{n - \sqrt{n^2 - NA^2}} \qquad\qquad \textbf{2.1}$$

Where **dz** is the section in the z direction, λ_{exc} is the excitation wavelength of the laser, **n** is the refractive index of the sample and **NA** is the numerical aperture. The Numerical Aperture of the Objective is the ratio of the radius of the objective to its distance (at its edge) from the object being observed, multiplied by the refractive index of the medium in which the object is situated. The resolving power of a microscope increases with increasing NA. This shows that the largest objective needs to be used in order to get the best confocal arrangement.

In these experiments the 50x objective (NA 0.85) was usually used, the slit set to 10 μm on the spectrograph entrance assembly and the CCD area set to a 4 pixel height, in contrast to a 20 μm slit width and a 20 pixel height for a non-confocal experiment. The thickness of the optical section can be defined as the Full Width at Half Maximum (FWHM) which can be seen below in Figure 2.6.

18

2000-

1500-

Intensity/
Arbitrary
units

1000-

500-

0-

20   10   0   -10   -20

Distance in z-direction/ micrometres

Figure 2.6   **Silicon sample, z-direction mapping, slits 10 μm, CCD pixel height 2, 50x objective. Static scan centred at 520 cm⁻¹, 10 sec scan. Scan taken every micron.**

The FWHM value of this peak is 3.38 μm; this shows the resolution of the instrument is 3.4 μm in the z-direction. This value alters though depending on the type of sample under investigation, the refractive index of the sample should be taken into account when trying to calculate the depth of a layer in a sample. This result makes it possible to calculate the optical section under investigation. This is calculated to be a 1 μm diameter x 3 μm cylinder in this instrument.

1 μm

3 μm
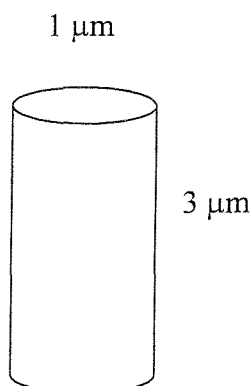
Figure 2.7   **Diagram to show the optical section under investigation with the confocal microscope.**

However as can be seen in equation 2.1 this value does depend on the refractive index of the sample hence the slice measured will be different for polystyrene and silicon. The calculated value for silicon (assuming a refractive index of 3.42 as measured by Edwards *et al*[22] in the infra-red) is 3.78 μm but the refractive index of polystyrene is 1.59 so the optical section in the z-direction will only be 1.7 μm when measuring the dry beads. Using the same calculation the optical section in the z-direction for a swollen bead will be 1.3 μm.

Figure 2.8 Summary of Optical slices calculated from the refractive indices.

| Sample	Refractive index	Optical slice in z-direction / μm
Silicon	3.42	3.8
Polystyrene[23]	1.59	1.7
Dioxane[23]	1.42	1.3

2.3 Bead Experiments

2.3.1 Loading Experiments

All Raman spectra were collected with a 632.8 nm (HeNe) laser on a Renishaw Raman imaging microscope 2000 system in the continuous extended grating mode using a grating of 1800 g mm^{-1}. In the normal mode of operation the slit width was 20 μm and the CCD array had an area of 20 x 577 pixels.

The spectra of the plain beads were collected with a x20 objective between 3500 cm^{-1} and 100 cm^{-1} with a 20-second exposure and 3 accumulations (approx. 45 mins, this is because in the extended scanning mode many exposures are required to complete the scan across the whole wavelength region.). The spectra of the loaded beads were collected with a x50 objective between 2300cm^{-1} and 900 cm^{-1} over a 20-second exposure and 10 accumulations (approx. 15 minutes).

The beads were mounted on a glass slide under the objective of the microscope for measurement. It was found that when measuring the swollen beads that the solvent evaporated extremely quickly, therefore the apparatus below was set up to prevent the solvent from evaporating in the experimental time scale.
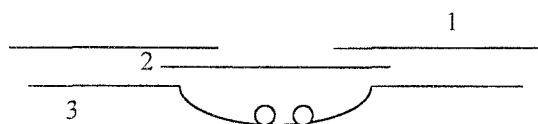
Figure 2.9   The arrangement of the glass slide. Key: 1 Parafilm, 2 Glass cover slip, 3 Glass microscope slide.

To reduce the solvent evaporation a glass cover slide was placed over the well of the glass slide and then a piece of parafilm stretched over this to keep the two pieces close together. To enable the beads to be seen through the objective a square piece of the parafilm was cut away with a knife. This arrangement (Figure 2.9) was used in all the experiments where the bead was swollen.

2.3.2 Line Mapping Experiments

The mapping experiments were always carried out in confocal mode. The slit width was set to 10 μm and the CCD array had an area of 4 x 577 pixels. A variable amount of scans were taken across the bead depending on its size and the time available. The spectra were collected with a x50 objective between 2300 cm^{-1} and 900 cm^{-1} to allow both the peak of interest (2232 cm^{-1}) and the reference polymer peak (1001 cm^{-1}) to be observed.

2.3.3 Area Mapping Experiments

These experiments were again carried out in confocal mode as described above, with a x50 objective. A static scan with a range of 453 cm^{-1} (with the 1800 Groove grating) centred at the peak of interest was used. The area is defined with the mapping software. The bead was focused manually on the bead centre and not with the auto-focus facility of the software, the xyz co-ordinates were always set to 0,0,0. It was decided to use the bi-directional scanning mode to avoid any jumps in the objective that may have caused the bead to move. For long scans (8 hours plus) 'cosmic ray removal' was turned on to remove large sporadic noise peaks disturbing the data.

The long-term stability of the bead was investigated by leaving the bead under the laser for two hours and spectra taken every 12 minutes. The change in intensity of the 1001 cm^{-1} peak over this time and no significant change was seen. If the polymer bead was melting one would expect the bands of the spectrum to broaden and the relative intensities of the bands to change, none of this was observable in the range of spectra. Black body emission within the spectra can also be seen when the sample heats but this again was not observed.

Our initial experiments experienced problems with the bead moving so to overcome this the bead was stuck to the microscope slide with paper glue. This also meant that it was not necessary to place a glass cover slide over the sample, as it was not going to move anywhere. It was also necessary to ensure that the white

light path and the laser path were exactly aligned otherwise when superimposing the map onto the picture of the bead a slight misalignment is observed. This was done by using a piece of silicon, when focused the laser spot is bright when viewed through the video viewer, it is necessary to have this centrally aligned around the crosshairs for the two light paths to be perfectly aligned.

2.3.4 Synthesis of Beads

The resin beads used for the measurements were prepared as follows: Aminomethylated polystyrene (0.040 g, 200-400 mesh, novabiochem) was placed in a 20 ml filtration funnel and swollen for 15 min in 9.3 ml of dioxane. The funnel was closed at the bottom with a little rubber stopper and on the top with a Suba-Seal septum. A solution of 0.023 g 4-Cyanobenzoic acid (Aldrich) and 24.4 μl of 1,3-Diisopropylcarbodiimide (DIC) in 700 μl of dioxane was freshly made up, left for two min and was then added to the pre-swollen resin. The reaction was quenched after the times given in the table. The stopper at the bottom was removed and the reaction mixture pressed through the filter by pushing the stamp of the air filled syringe. Immediately after that the sample was flushed with 20 ml of dioxane which was delivered from the second syringe on top of the reaction vessel. Then the resin was washed with 20 ml of dichloromethane (DCM), 20 ml of MeOH and 20 ml of Et$_2$O and dried for two hours in high vacuum.
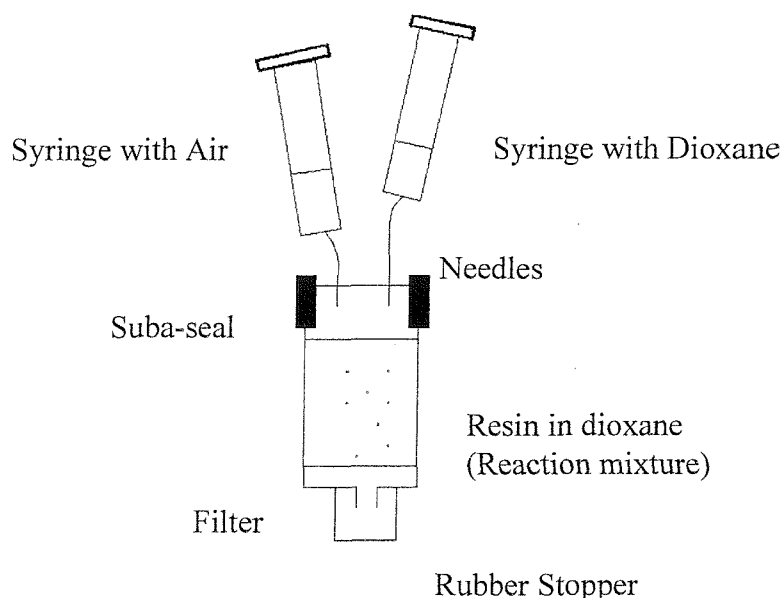
Figure 2.10   Diagram to show the synthesis of the Loaded Beads

Table 2.1 Table to show the ninhydrin substitution and loading of beads.

Time / min	Substitution / Ninhydrin tests mmol g^{-1}	Loading / %
0	1.310	0
0.5	0.899	31
1	0.751	43
2	0.582	56
4	0.449	66
6	0.329	75
8	0.261	80
20	0.159	88
30	0.180	86
40	0.123	91
50	0.062	95

The ninhydrin tests were carried out as follows: A certain amount of the resin (2-6 mg) was weighed into a small test tube. Twelve drops of a stock solution A and six drops of a stock solution B were added to the resin and the suspension left at 100 °C in a heating block for 7 min. The stock solutions were available in the laboratory, prepared according to literature [24]. The suspension was filtered through glass wool into a 50 ml volumetric flask, washed thoroughly with EtOH / H_2O (60 / 40) and four times with 600 µl of a 0.5 molar solution of tetraethylammonium chloride hydrate (Aldrich) in DCM. The solution was made up to 50 ml with EtOH / H_2O. The UV-Vis spectrum of this solution was measured against a blind. The absorption at 570 nm is recorded and used in the following formula:

Substitution = Absorbance at 570 nm x 50000 / 15000 x mass of resin in mg

The loading of the resin is given by the following equation:

Loading = 100 - Substitution x 100 / 1.31

Therefore the substitution of the unloaded resin was established to be 1.31 mmol g^{-1}.

2.4 Analysis

The spectra of the loaded beads were analysed using the GRAMS curve fitting application. The 2332 cm^{-1} peak due to the CN stretch of the cyanobenzamide and the 1001 cm^{-1} peak due to the mono-substituted aromatic ring breathing mode of the polymer were curve fitted with a mixture of Gaussian and Lorentzian curves and the ratio of the peak areas are taken to allow instrumental response. The mapping results were analysed in a similar way. The mapping results are in the format of a multifile so that the curve fitting parameters can be applied to all the separate files. The maps are created using the mapping program supplied with the WiRE™ (Windows-based Raman Environment) program from Renishaw. The maps are displayed as bitmaps with the scale adjusting to have the best fit for the data.

This work was undertaken in collaboration with Dr Jürgen Kress of Southampton University.

2.5 Atomic Force Microscopy

The atomic force microscopy experiments were carried out to support the lens effect theory (this will be discussed further in the discussion, section 4). The instrument used was a Burleigh vista scanning probe microscope, the instrument was used in AC mode AFM (Tapping mode AFM), with tip length 10-15 μm, aspect ratio of 1:1, the radius at the end of the silicon tip was 10 nm. The cantilever was a 7 μm thick rectangle of dimensions 219 x 45 μm. The force constant was 30-50 Nm^{-1} and resonant frequency 150-250 kHz. The 0.31 mm thick carrier was a 3.6 x 1.6 mm rectangle and had a 35.3 ° angle of edge bevel.

The beads measured were 73% loaded and measured in the dry state, it was difficult to find a bead that did not become attached to the tip and vibrate with it. The tip was manoeuvred into place with the help of a video camera, this also aided knowing whether the bead was moving with the tip.

3   RESULTS AND ANALYSIS

This investigation started by looking at several types of beads and collecting the Raman spectra, then went on to load the beads with 4-cyanobenzoic acid and look at the change in the spectra with loading. This lead onto the investigations into the structure of the beads by using the cyanobenzamide tag as a bead, the various maps obtained are presented.

3.1   Raman Spectroscopy of Beads

3.1.1   Aminomethylated Polystyrene Resin

In this section the spectra of three different beads commonly used in solid-phase synthesis are presented. The structures of these are shown below.
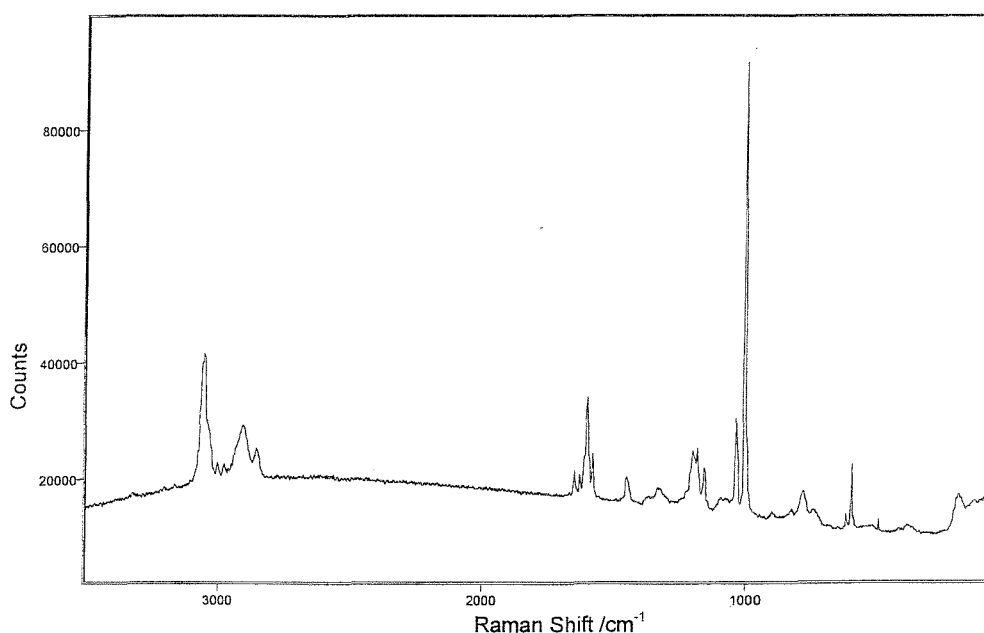
Figure 3.1   **Spectrum of an aminomethylated polystyrene bead, 2 accumulations, 20 seconds exposure.**

The structure of the polymer is shown below in
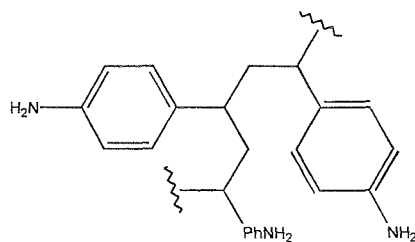
**Figure 3.2**   **Structure of Aminomethylated Polystyrene**

This spectrum shows a typical polystyrene spectrum. The main assignments of the peaks are shown below.

Table 3.1 Main Assignments of Peaks in an Aminomethylated Polystyrene Bead

Raman Shift /cm^{-1}	Assignment
621	Ring deformation
1001	Ring breathing
1450	CH$_3$ deformations
1583-1649	Ring stretches
2854-2950	Antisymmetric CH$_2$ stretch
3055	Aromatic CH stretch

The spectra show that there is vibrational structure from 2800 cm^{-1} to 3200 cm^{-1} due to the CH$_2$ groups in the polymer and 1600 cm^{-1} to 600 cm^{-1} due mainly to the aromatic rings in the structure. The peaks are strong and the spectrum has a little noise and shows no fluorescence, which would deviate the baseline from horizontal.
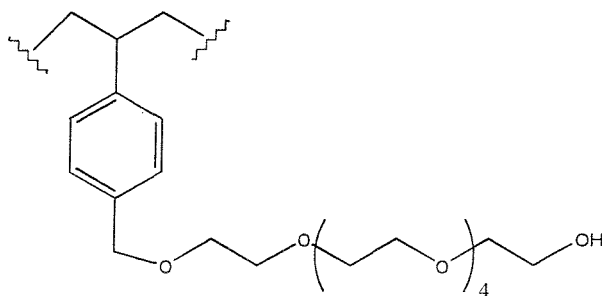
3.1.2 TentaGel Resin
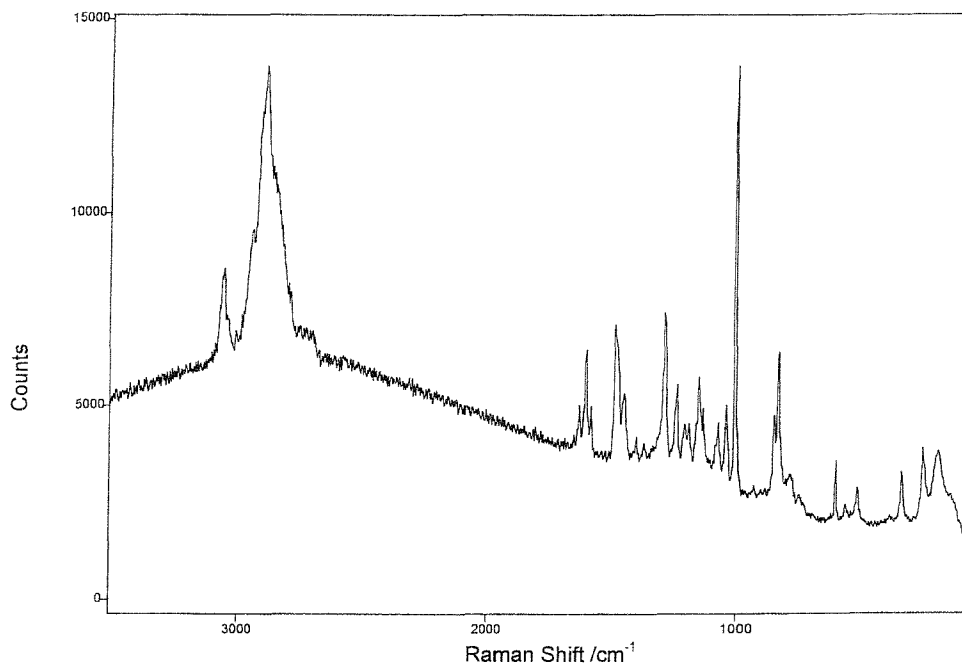
Figure 3.3 Spectrum of TentaGel Bead, 3 accumulations, 20 seconds exposure.

The structure of Tentagel is shown below, it is a polystyrene resin with ethylene glycol functionality attached.

Figure 3.4   Structure of Tentagel Resin

The assignments of the main peaks can been seen below.

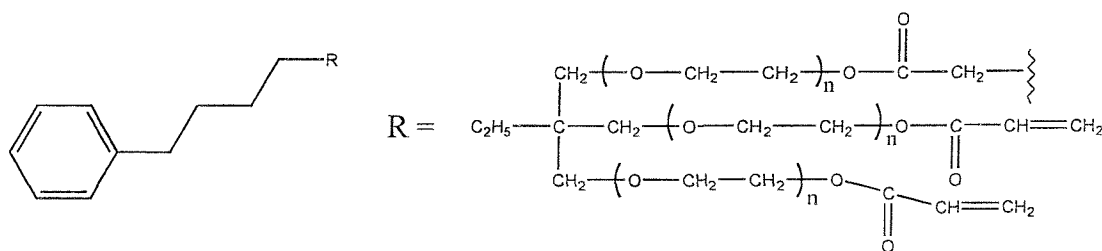**Table 3.2   Main Assignments of Peaks in an TentaGel Bead**

Raman Shift /cm^{-1}	Assignment
1031	Ring breathing
1280	Ring stretch
1603	Ring stretch
2885	CH stretch
3055	Aromatic CH stretch

3.1.3 Clear Resin
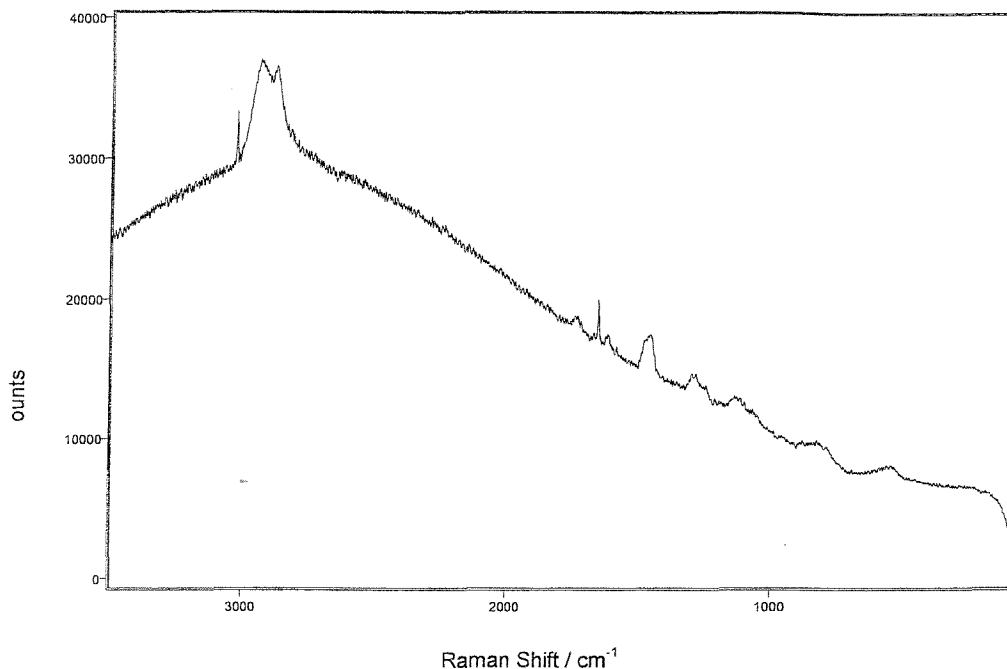
Figure 3.5   **Spectrum of Clear Resin, 2 accumulations, 20 seconds exposure.**

Clear is an acronym for Cross Linked Epoxy Acrylic Resins and has the structure shown in Figure 3.6

Figure 3.6   **Molecular structure of Clear beads.**

Table 3.3   **Main Assignments of Peaks in a Clear bead**

Raman Shift /cm^{-1}	Assignment
1582	Ring stretches
1649	C=C stretch
2879	Symmetric CH$_2$ stretch

The structure of the clear beads contains many CH$_2$ groups, which is why a large peak is observed in the spectrum. The spectrum shows that the bead fluoresces, as the baseline is non-linear. The spectrum does not have clearly defined peaks.

29

3.1.4 Analysis of bead types

After analysis of the 3 main bead types it was decided that the aminomethylated polystyrene resin had the better Raman spectrum out of the three different resins for the definition of the nitrile stretch (v_{CN}). This was decided because it had a flat baseline and clearly defined peaks. TentaGel resin also showed these attributes but had a more complex vibrational structure; therefore it was decided that the rest of the studies would be performed with aminomethylated polystyrene resin.

3.2 Loading Experiments

On inspection of the aminomethylated polystyrene spectrum we noticed that there was a region from 1612 cm^{-1} to 2720 cm^{-1} where no peaks were observed. After looking for functional groups that showed a strong Raman vibration in this area it was decided that 4-cyanobenzoic acid would be loaded onto the bead as it was expected to show a strong peak at 2232 cm^{-1} for the v_{CN}. This was observed for both dry and swollen beads and at higher loadings a more intense peak was seen as shown in
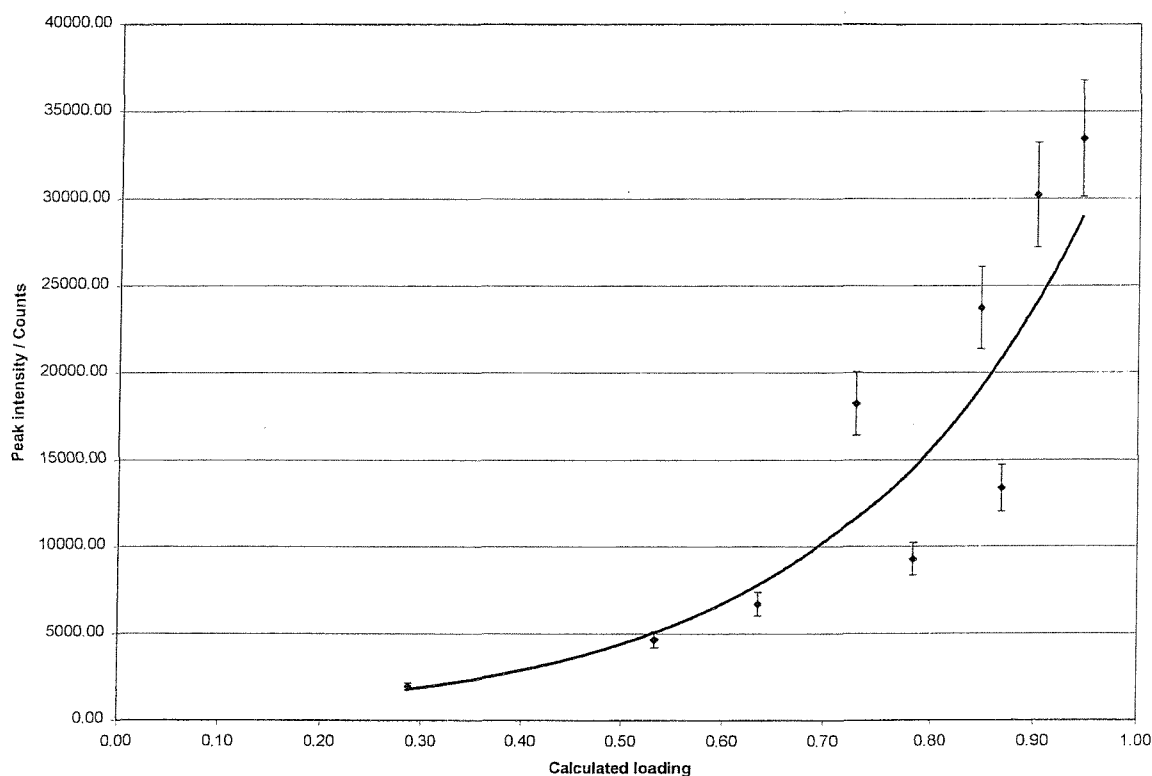
Figure 3.7.
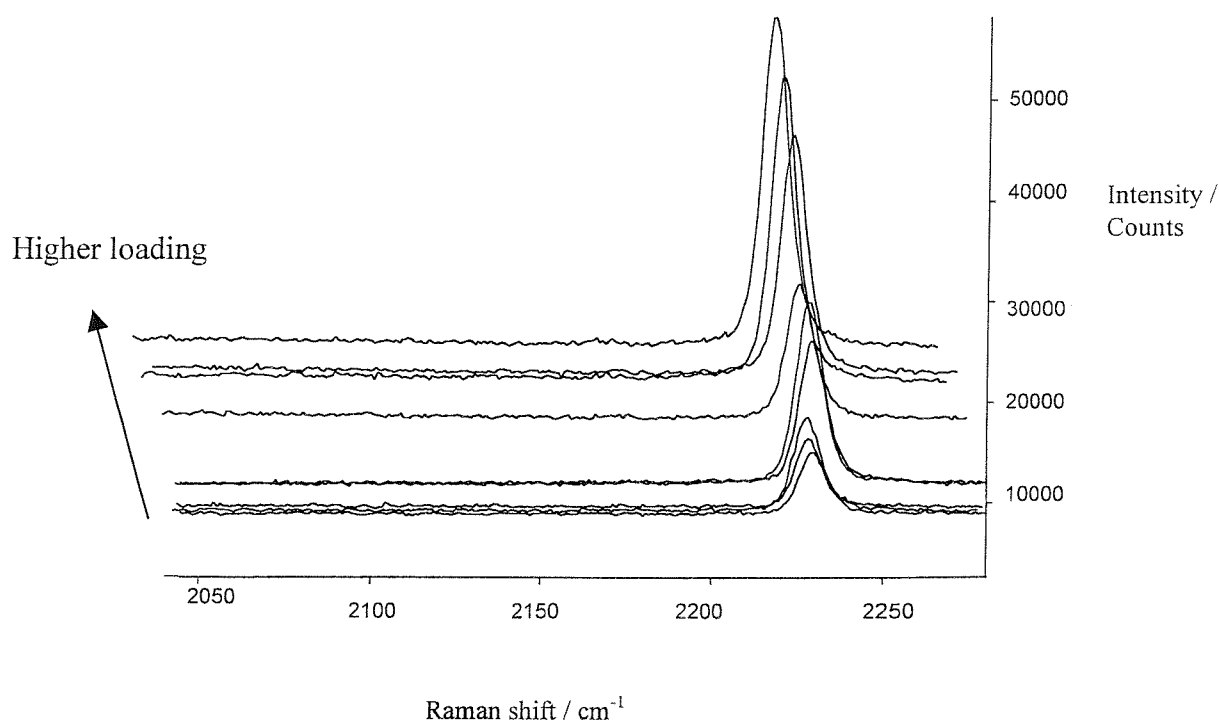
Figure 3.7   **Figure showing the increasing peak intensity against loading for a dry bead.**
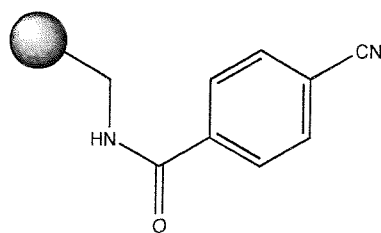
Figure 3.8   Molecular structure of 4-cyanobenzoic acid attached to the resin.

3.2.1   Loading on Dry Beads

The peak intensity was plotted against the loading to discover the relationship between the two.

Figure 3.9   Graph to show the Peak Intensity against the calculated loading for dry beads.

This graph shows a non-linear dependence between the calculated loading and the peak intensity. It is the calculated loading that is plotted against the intensity, due to the procedure that is used to calculate the loading from the Ninhydrin test (see section 3.2.5). The data for these plots is obtained from the 'curve fit' function of

the WiRE software. Each peak was curve fitted and the parameters obtained used. The errors from these parameters have been used to add error bars to these plots.
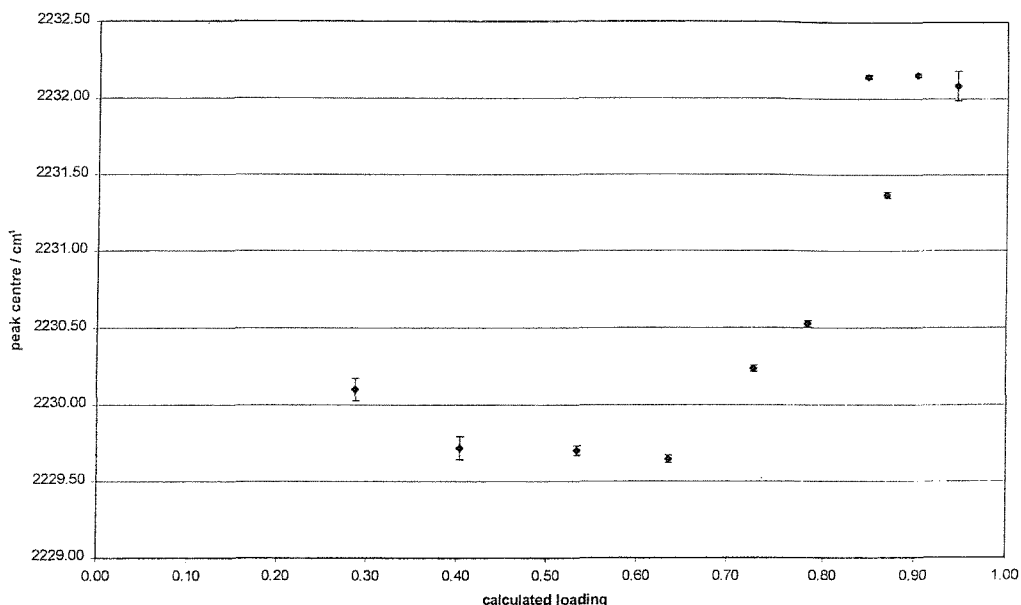
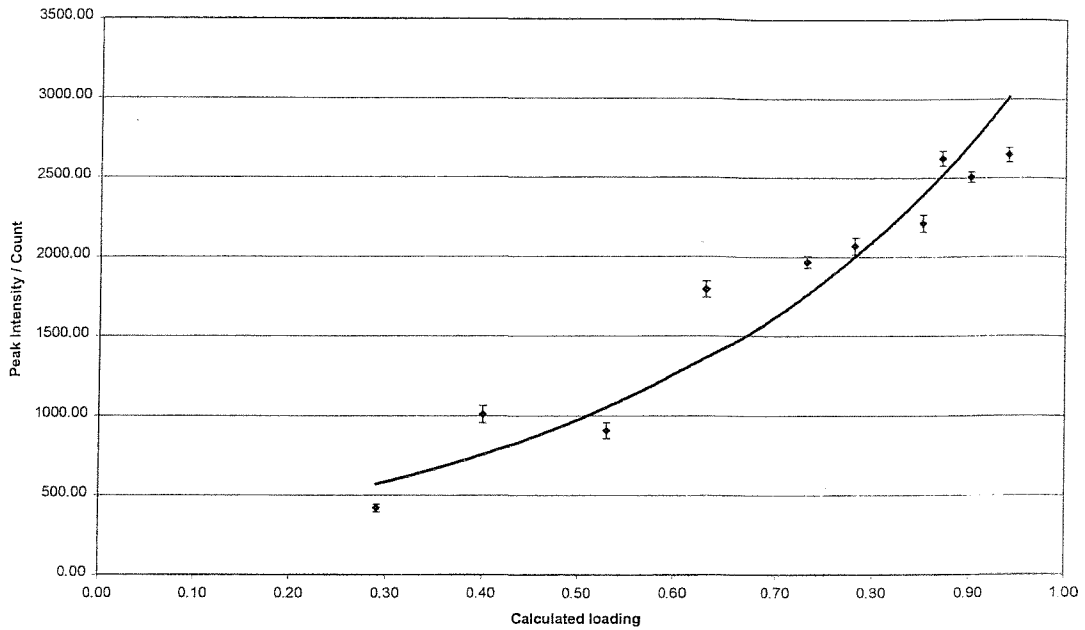**Figure 3.10   Graph to show the relationship between peak centre and loading.**

This graph shows that there is a non-linear relationship between peak centre and the loading of cyanobenzoic acid. At lower loading v_{CN} is at ~2229 cm^{-1} and it increases steadily until at higher loading it is at ~ 2232 cm^{-1}. The data point at 0.29 calculated loading does not fit the trend of the graph, this bead was measured first therefore the instrument may not have been perfectly warmed up and produced this bad data point, which should be ignored. Other measurements taken of different sets of beads showed a trend towards higher wavenumber for more heavily loaded beads. It would be expected for the peak centre to remain unchanged if the environment inside the bead didn't alter, it is known that the peak position of dyes is affected by the polarity of the solvent, which is an environmental effect.

3.2.2   Analysis of Loading for Dry Beads

The relationship between peak intensity and loading is best described by a curve, we expected that the relationship would be linear, so to discover why this curve

was seen I looked further into the results. I discovered that there is a relationship between the peak centre of the ν_{CN} and the loading of the bead, this may indicate why a non-linear relationship is seen between the peak intensity and loading. These ideas will be expanded more in section 3.3.

3.2.3 Loading on Swollen Beads

Figure 3.11   Graph to show the Peak Intensity against the Calculated loading for swollen beads.

This graph shows a non-linear dependence on loading for peak intensity on a swollen bead. The error bars are calculated from the standard error on the curve fitting for each on the different beads. The error is fairly standard for the whole of the sample and is about 5 % of the value.
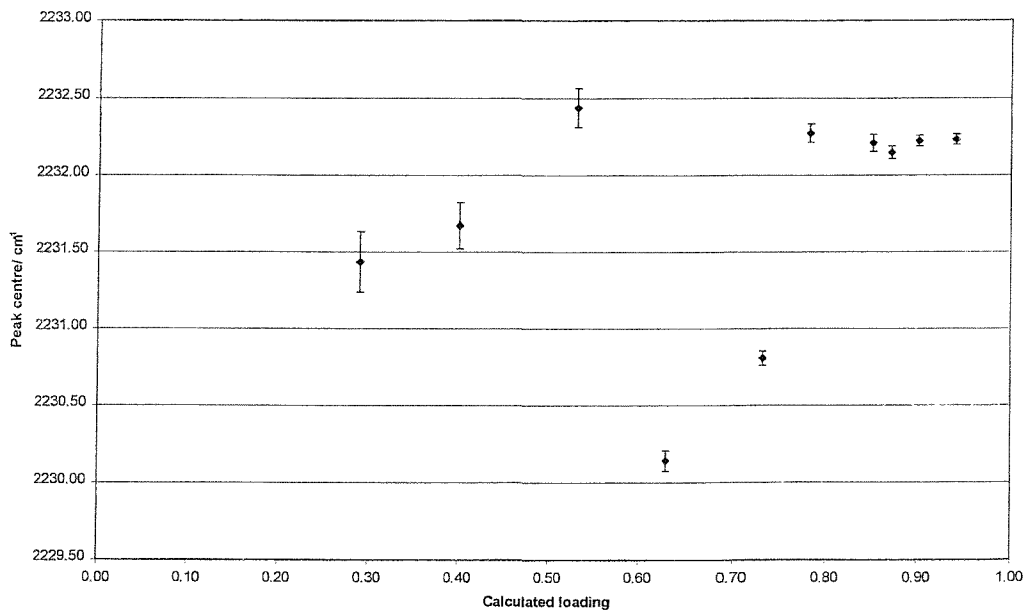
Figure 3.12   Graph to show the relationship between peak centre and loading for swollen beads.

34

This graph shows an almost random distribution of peak centres for swollen beads, the later data points (loading >0.8) all show about the same value, 2232.25 cm^{-1}. The data points below this are at lower wavenumbers and the first three data points increase steadily between 2231.5 cm^{-1} and 2232.5 cm^{-1}. Larger error bars are seen on the beads with lower loading, this is due to the higher signal to noise ration for these samples. At lower loading a smaller peak is seen therefore the signal to noise ratio will be lower than that of the higher loaded beads.

3.2.4   Analysis of Loading for Swollen Beads

Again a non-linear relationship was seen between the calculated loading and the peak intensity in a swollen bead, this distribution is more linear than the one seen for a dry bead but could not be described by a straight line. When the peak centre is plotted against the calculated loading an almost random relationship is observed as opposed to that of the dry bead where a steady increase was found in the peak centre with loading. In the swollen bead the highest loaded beads also have the largest wavenumber value of the set but a gradual increase is not seen, the beads loaded with 63 % and 73% have peak centres well below the trend.

3.2.5   Calculation of Loading from Ninhydrin Tests

In the ninhydrin test the loading of a loaded bead is compared to that of an unloaded bead. The ninhydrin attaches itself to all the available sites and this is then used as the standard from which the loading of the loaded beads is calculated per mass of bead. Therefore if a large pendant group is attached fewer beads will actually be used to calculate the loading and this will skew the actual loading of the beads. To calculate the loading per bead (as opposed per mass of bead) the equations below were developed which calculate the actual loading of a bead from the result of the ninhydrin test.

Mass of a bead = M   Number of occupied sites = n

Number of sites per bead = N   Mass of attached group = m

$$Loading = \frac{\text{No. of occupied sites per bead}}{\text{Total no. of sites per bead}} = \frac{n}{N} \qquad \textbf{3.1}$$

The test determines the number of free sites per unit mass of a selection of beads.

$$\text{Original bead} = f_o = \frac{N}{M} \qquad \textbf{3.2}$$

$$\text{Loaded bead} = f = \frac{(N-n)}{(M+nm)} \qquad \textbf{3.3}$$

The calculated loading is the number is of loaded sites per unit mass. It is the number of free sites per unit mass of the original bead minus the number of loaded sites on the bead per unit mass.

$$\delta = f_o - f = \frac{N}{M} - \frac{(N-n)}{(M+nm)}$$

$$= \frac{N(M+nm) - M(N-n)}{M(M+nm)}$$

$$= \frac{nNm + Mn}{M(M+nm)}$$

$$= \frac{n(M+mN}{M(M+nm)} \qquad \textbf{3.4}$$

$$\text{Calculated loading} = L' = \frac{\delta \times M}{N} \qquad \textbf{3.5}$$

$$= \frac{n(M+mN)}{M(M+nm)} \times \frac{M}{N}$$

$$= \left(\frac{n}{N}\right) \times \frac{(M+mN)}{(M+nm)}$$

$$L' = L \times \frac{(M+mN)}{(M+nm)} \qquad \textbf{3.6}$$

$$M + mN = \text{mass of a fully loaded bead} = M_{100} \qquad \textbf{3.7}$$

$$L = L' \times \frac{(M + nm)}{(M + mN)} = L' \times \frac{(M + nm)}{M_{100}} \qquad \textbf{3.8}$$

$$= \frac{L' \times \left(M + \dfrac{n}{N} \times Nm\right)}{M_{100}}$$

$$= \frac{L'(M + L \times Nm)}{M_{100}}$$

Nm   = mass of the attached groups for a fully loaded bead

$$= M_{100} - M$$

$$= M_a$$

$$L = \frac{L'(M + LM_a)}{M_{100}} \qquad \textbf{3.9}$$

This can be rearranged to give:

$$L = \frac{L' M_a}{M_{100} - L' M_a} \qquad \textbf{3.10}$$

Where

M_a is the mass of the functional group loaded (g)

L' is the loading from Ninhydrin tests

L is True Fractional loading

M is the mass of an unloaded bead (g)

M_{100} is the mass of a fully loaded bead.(g)

As the cyanobenzoic acid has a mass of only 1.12×10^{-6} g on a fully loaded bead it does not effect the loading value significantly but a larger pendant molecule could.

**Table 3.4   Table to show how the mass of the pendant group affects loading.**

L' Ninhydrin	M Mass of empty bead	M_{100}	L actual
0.8	0.000001	1.12×10^{-6}	0.78
		1.3×10^{-6}	0.75

As can been seen from the table above, the calculations alter the true loading for cyanobenzamide by only 2 % but with a larger pendant group this could be more significant, by changing the mass to only about three times as large the loading is altered by 5 %.

3.3   Bead Distribution

To investigate the significance of the curve observed for the peak intensity against loading chart, distributions of beads in a random set of twenty were measured. I looked at three bead samples with different loadings; 29 %, 73% and 94 % loaded beads.
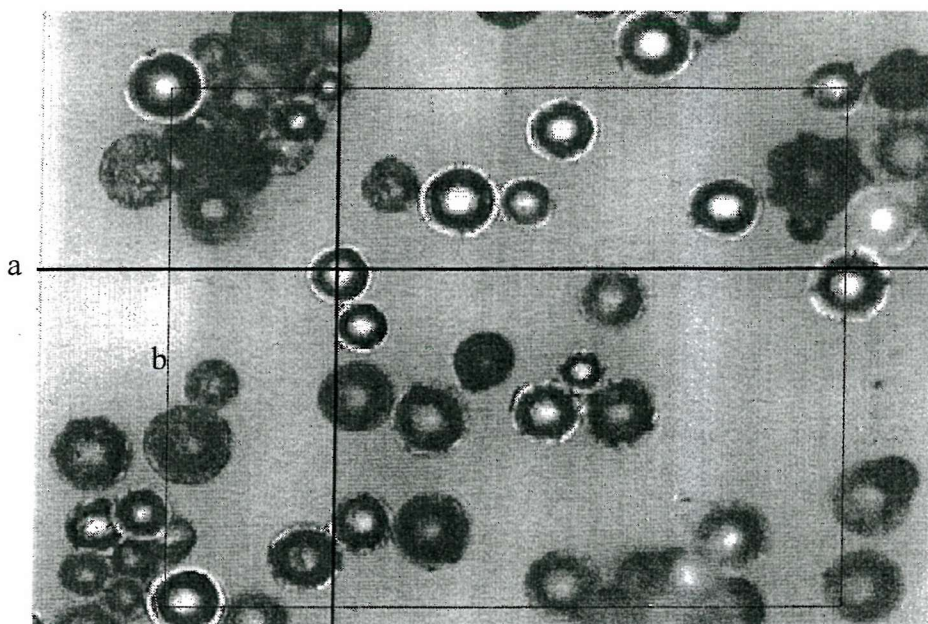
Figure 3.13   Picture to show how the beads were selected for sampling. 10 beads were selected in this set. Key: a: crosshairs, b: area selected around 10 beads.

From this picture it is easy to see the variance in the beads, from their size to their transparency. Ten beads were selected at random from this set of beads and the Raman spectrum collected from the middle of each selected bead. This process was repeated with another set of randomly selected beads so as to have a sample of 20 beads to analyse.

3.3.1 Histograms of Bead Intensity
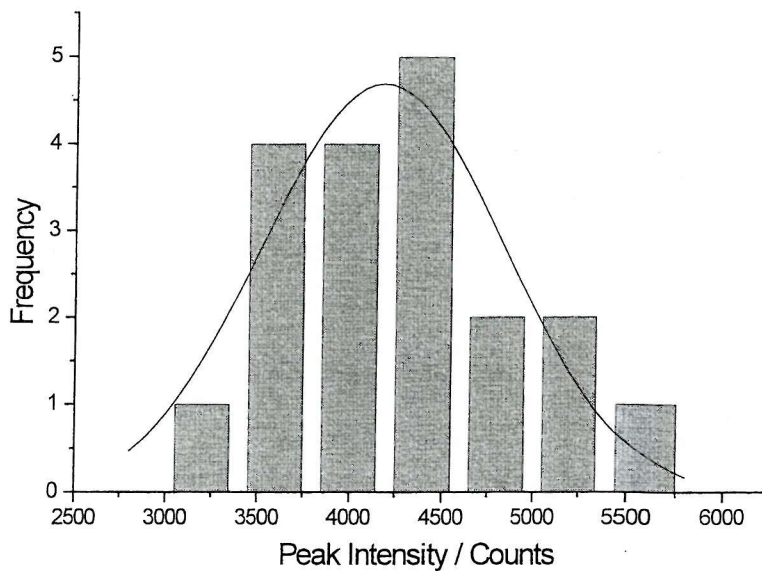
Figure 3.14 **Histogram to show the variation in peak intensity in a set of 20 beads with 29 % loading**
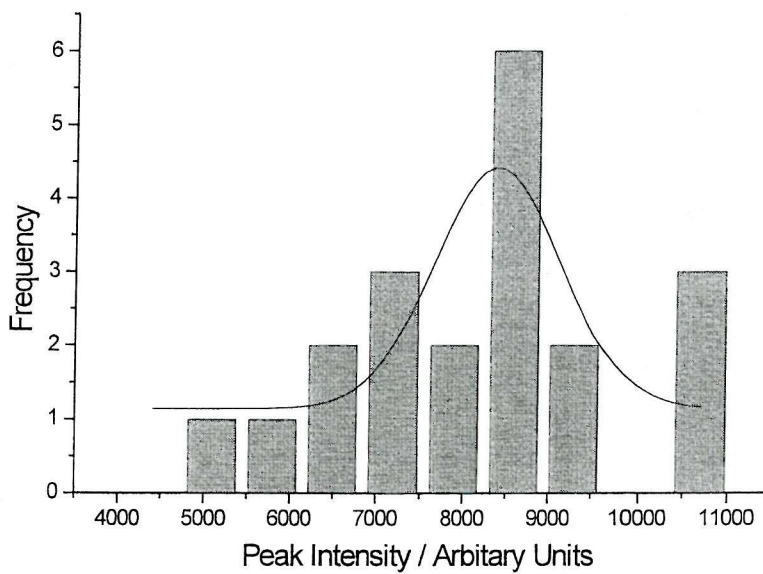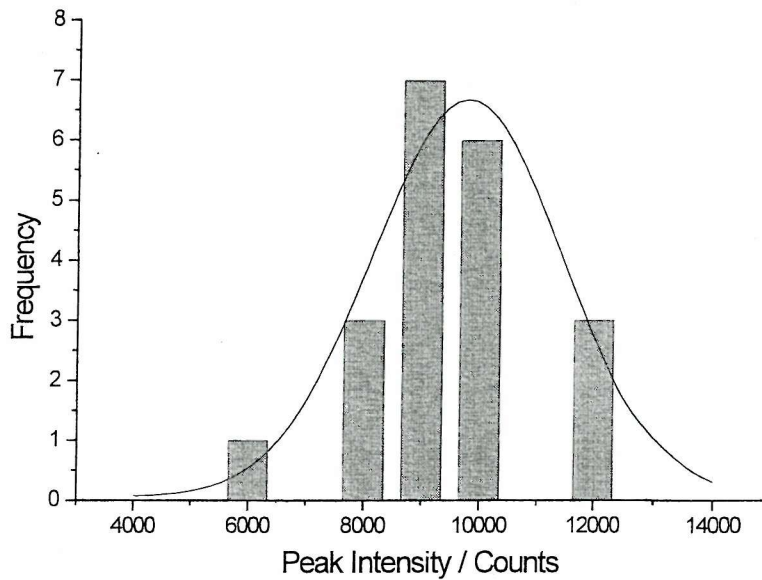

Figure 3.15 **Histogram to show the variation in peak intensity in a set of 20 beads with 73 % loading.**

Figure 3.16 **Histogram to show the variation in peak intensity in a set of 20 beads with 94 % loading.**

Table 3.5 **Table to show statistical data associated with the above graphs.**

| Loading / %	Average intensity	Standard deviation	Standard error	Percentage spread from mean / %
29	3915	803	180	21
73	7852	1629	364	21
94	8670	1397	312	16

3.3.2 Analysis of Histograms of Peak Intensity

All three histograms show that the sample of beads taken fit a Gaussian curve when plotted as a histogram. The beads with 73 % loading show the worst fit to the Gaussian curve, this is also shown in the statistical data above (Table 3.5), the 73 % bead has the highest standard deviation of the 3 sample. The histogram is useful as it shows the frequency of beads in a range of peak intensities. The low and high loaded beads (29 % and 94 % respectively) show a spread of peak intensities but with several beads contained in each range of intensities. The bead with average loading (73 %) shows a wide range of intensities with the data being quite dispersed throughout these, hence the large standard deviation and poor Gaussian

fit. The 29 % sample of beads show the best fit, the standard deviation is low, showing a low spread of peak intensities.

3.3.3 Histograms of Peak Centre Position

To discover whether the relationship between peak centre and loading was relevant the distribution in peak centres of the same samples of beads was analysed. The results are shown below.
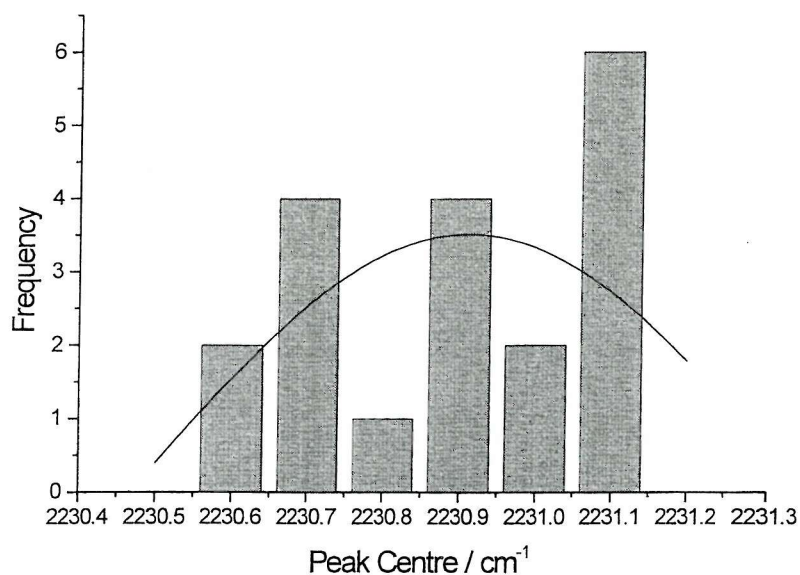
Figure 3.17 **Histogram to show the variation in peak ν_{CN} in a set of 20 beads with 29 % loading.**
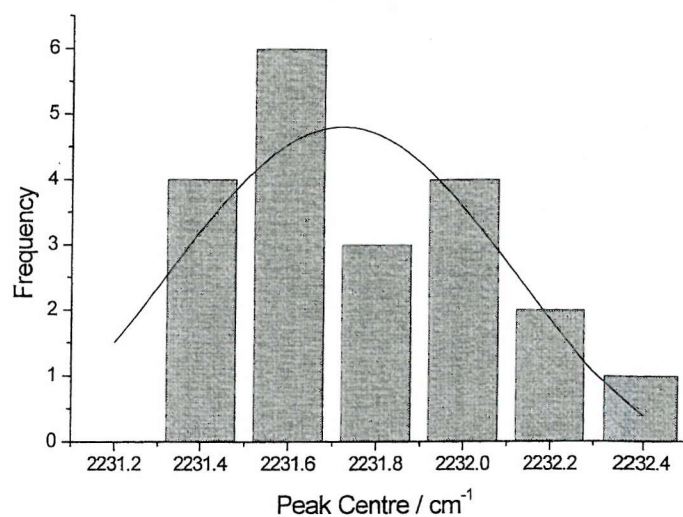
Figure 3.18 **Histogram to show the variation in peak ν_{CN} in a set of 20 beads with 73 % loading.**
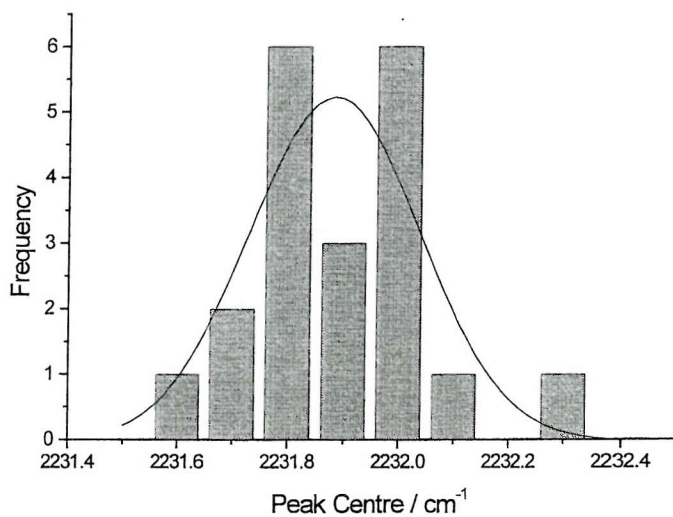
Figure 3.19 **Histogram to show the variation in peak ν_{CN} in a set of 20 beads with 94 % loading.**

Table 3.6   **Table to show statistical data associated with the above graphs.**

Loading / %	Average peak centre / cm^{-1}	Standard deviation	Standard error of the mean.
29	2230.85	0.18	0.042
73	2231.68	0.28	0.062
94	2231.85	0.13	0.028

3.3.4   Analysis of Histograms of Peak Centre

The data shown in the above graphs shows that there is quite a distribution from the mean in the peak centres at a given loading. The 29 % loaded bead shows the poorest fit to a Gaussian curve although this same spread is not observed in the statistical data. The statistical data shows that the 73 % loaded bead sample has the beads with the widest range of peak centres, as it has the highest standard deviation and standard error figures. The graph shows that the fit for the Gaussian curve is better than that for the 29 % loaded sample. The 94 % loaded bead has the best fit to the Gaussian curve, this is borne out also in the statistical data as the lowest standard deviation and standard error figures are shown.

3.4 Line Mapping

To look at the structure of the beads using 4-cyanobenzamide as a probe we started by doing line-mapping experiments. Line mapping experiments reveal more details about the internal structure of the beads. This consisted of taking a spectrum at regular intervals across the bead in the x or z direction. Examples of these are shown below.
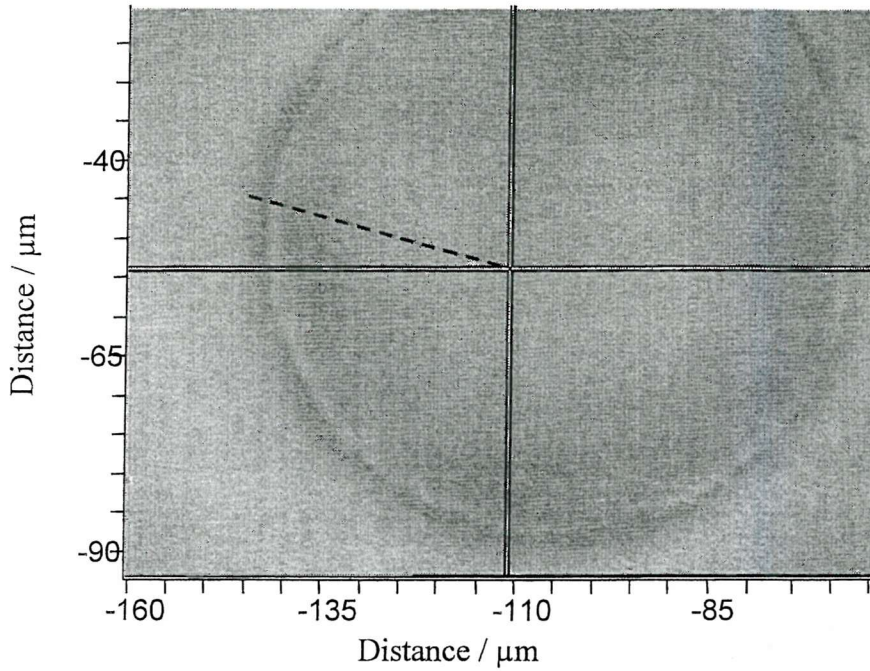

Figure 3.20 Example of the section selected for line mapping.
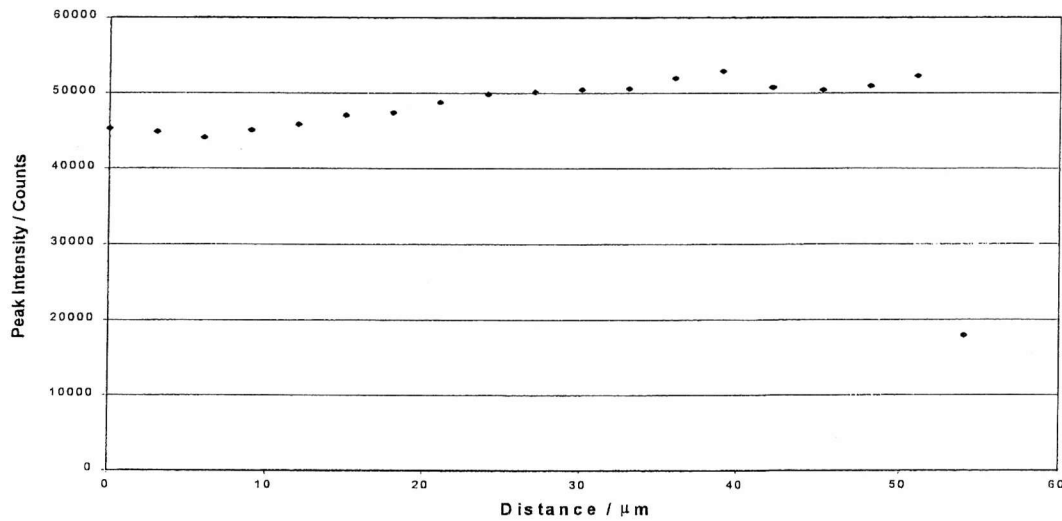**– – – – Area sampled**

Figure 3.21 x-direction mapping of a dry bead with loading of 70 %.
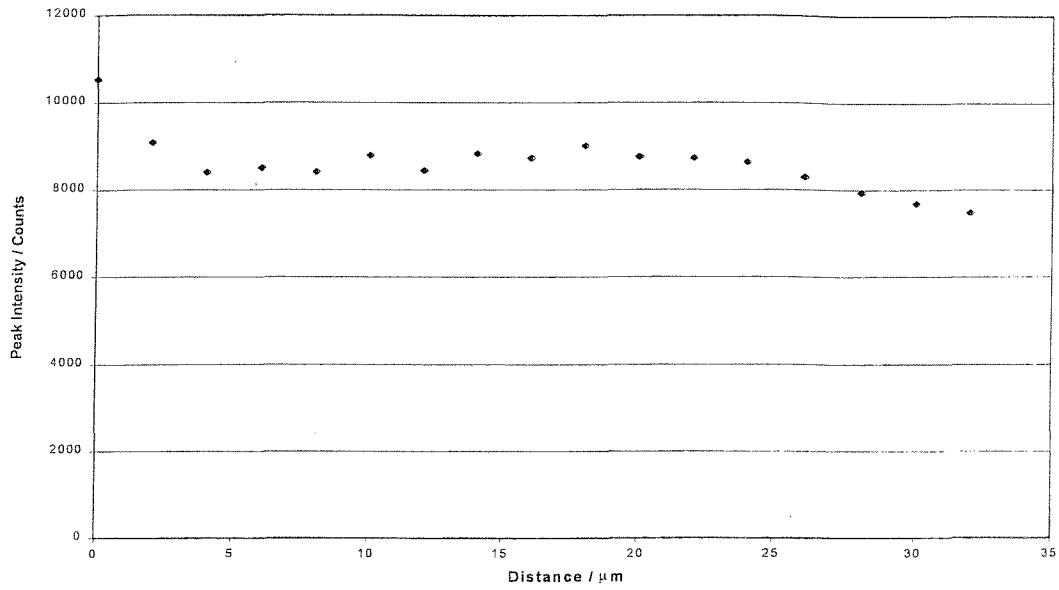
3.4.1 Dry Beads

Figure 3.22 x-direction mapping for a dry bead with loading of 90 %

3.4.2 Swollen Beads
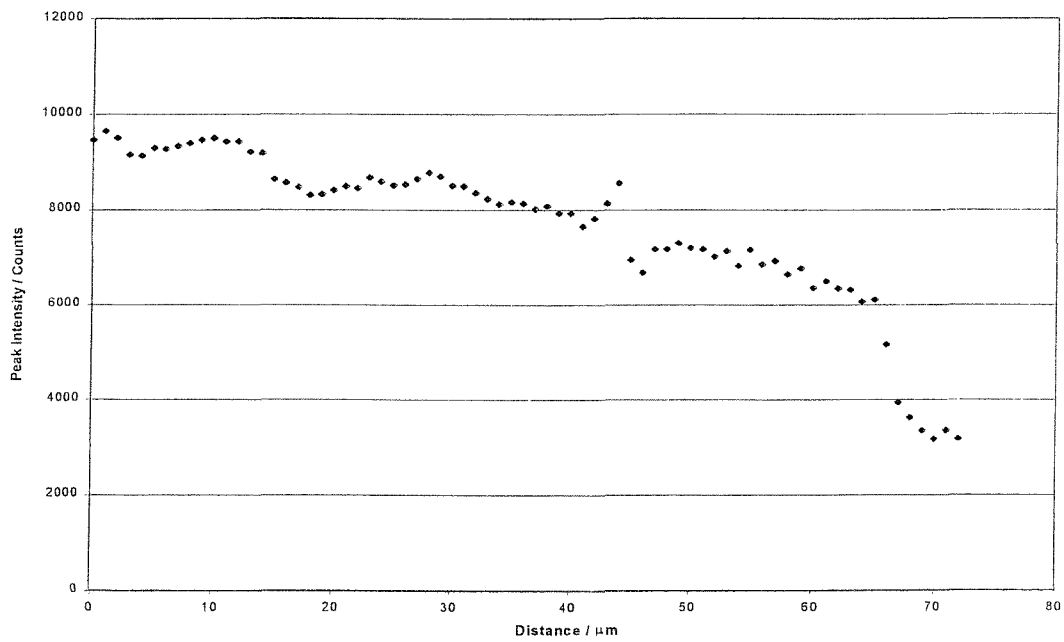
Figure 3.23 x-direction mapping of a swollen bead with 80 % loading.
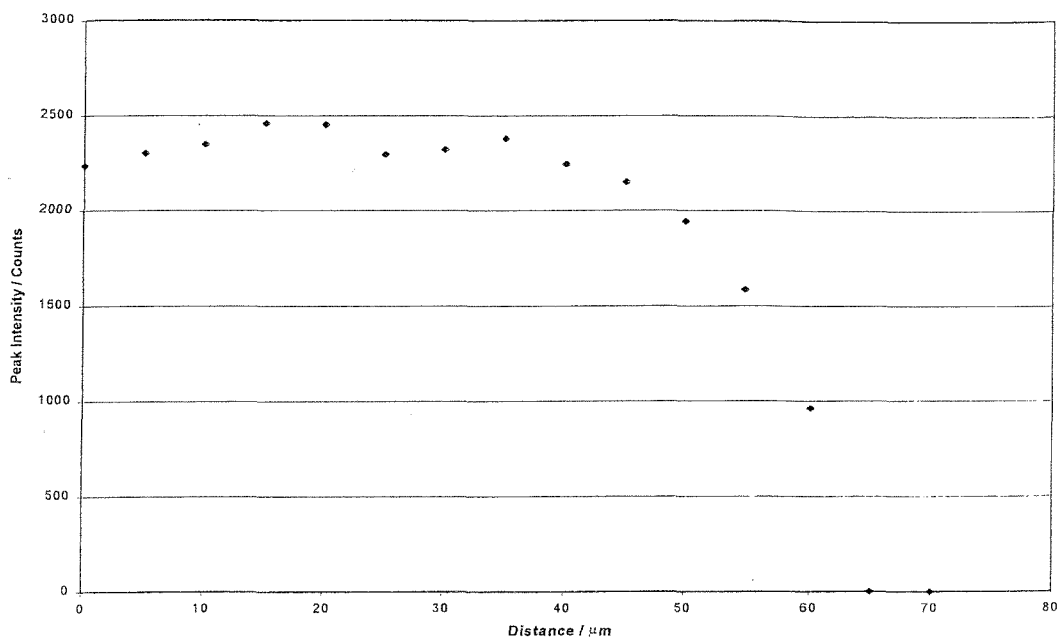
Figure 3.24   x-direction mapping of a swollen bead with 100% loading

3.4.3   Analysis of line mapping results

These results show that for both dry and swollen beads a similar pattern is shown when the beads are mapped from the centre of them to the outside. On all the graphs zero represents the middle of the bead and the maps run towards the outside of the bead. The maps show the levels of cyanobenzamide being constant throughout the bulk of the bead, where the data drops towards zero is where the mapping ran over the edge of the bead and hence there was no cyanobenzamide present. In Figure 3.21 this is only seen for the last data point and in Figure 3.22 the whole of the map was inside the bead, as the data remains constant throughout the graph. In Figure 3.23 there is a steady decrease in the level of cyanobenzamide towards the edge of the bead and from the graph it is possible to tell that the edge of the bead was at about 65 microns. In Figure 3.24 the data drops to zero for the last two data points, the edge of the bead is probably at 60 microns as a lower level of the tag is observed here.

3.5 Depth Mapping

Depth measurements were performed on the beads to ensure that what was seen in the x-direction was also see in the z-direction. This method also shows how effectively the confocal Raman microscope works, as it is possible to see the bottom of the bead.

Figure 3.25   **z-direction map for both polymer peak, 1001 cm^{-1} (square) and v_{CN} (triangle) on a swollen bead.**

This figure shows how both the $v_{polymer}$ and v_{CN} are found in exactly the same places on the bead. The data is set on opposite axes due to the differing intensities of the two peaks. It is possible to see the dip that appears in the polymer at the top of the chart also appears in the v_{CN} data.

3.5.1 Dry Beads
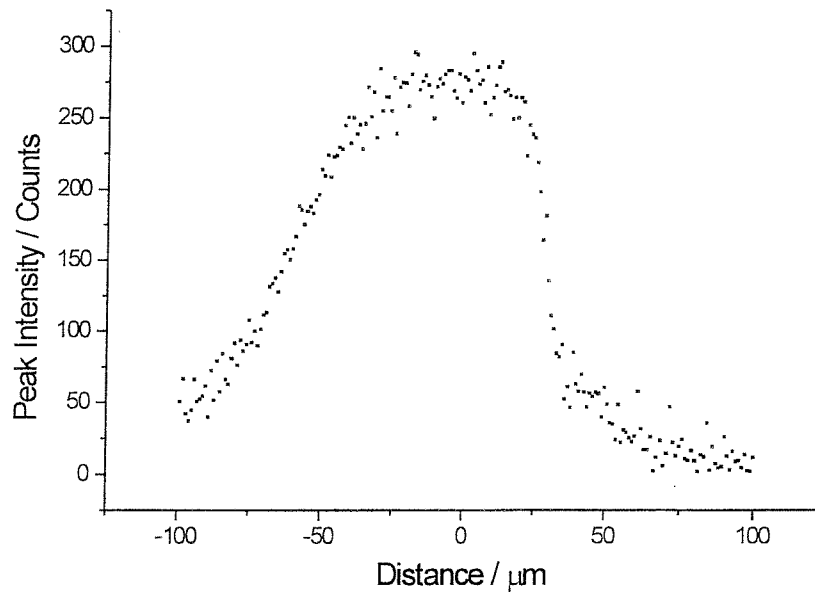
Figure 3.26 z-direction mapping of a dry bead with 94 % loading.

3.5.2 Swollen bead

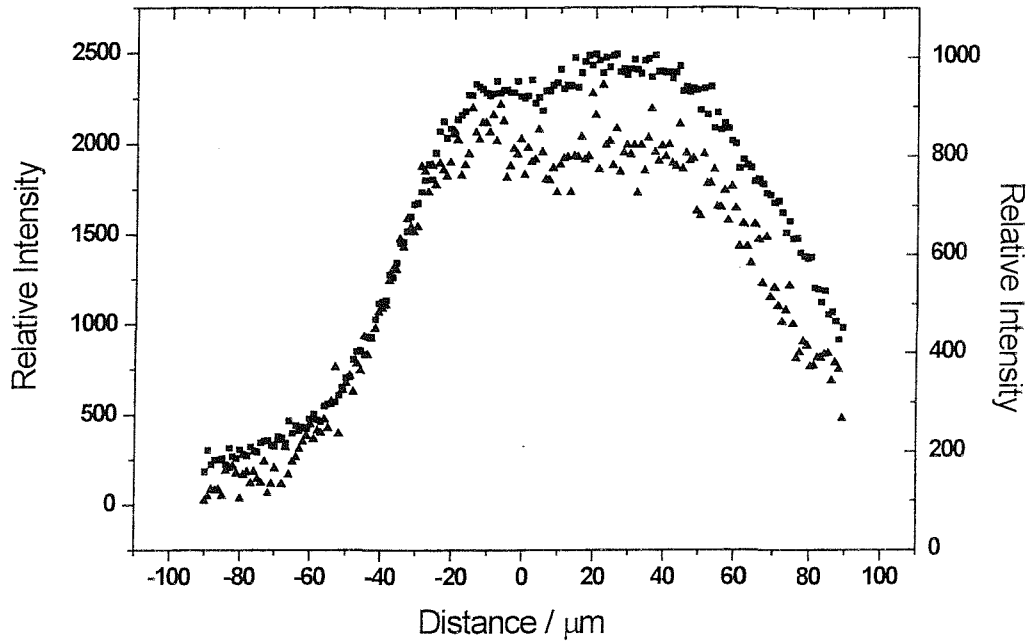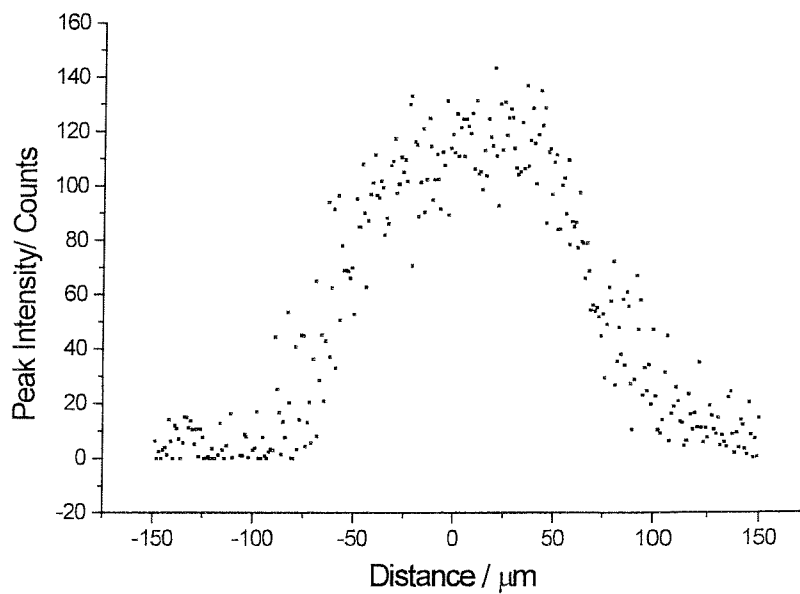**Figure 3.27 z-direction mapping of a swollen bead with 94 % loading.**
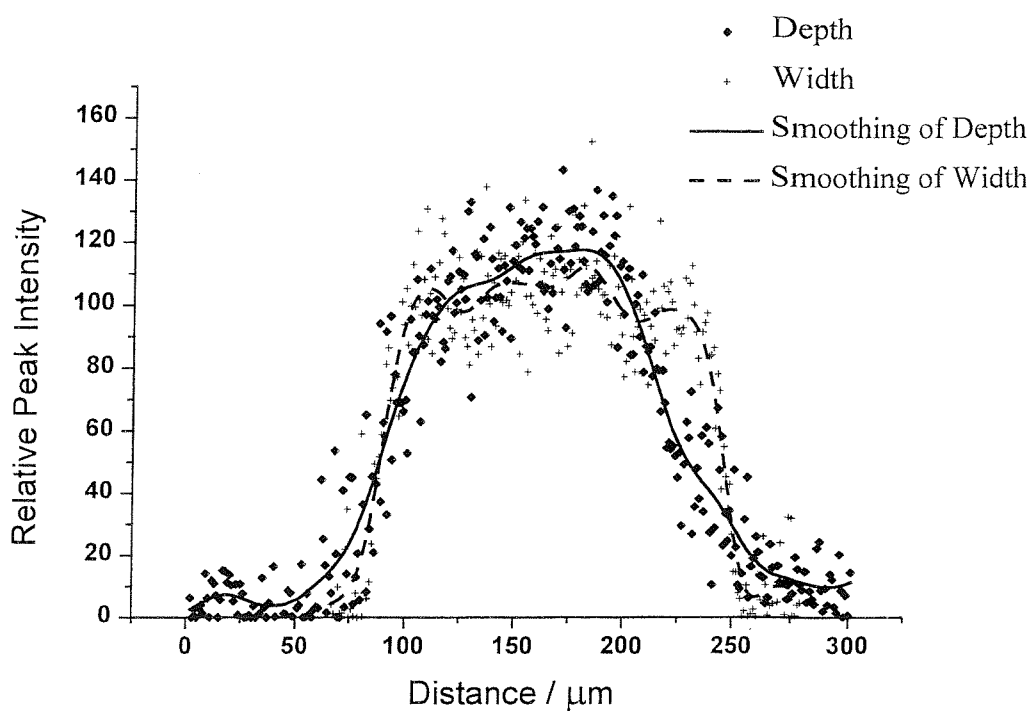
Figure 3.28 Depth and Width confocal mapping of the same swollen bead.

This figure shows the bead when it is mapped in the xy plane (width) and in the z-axis (depth). The data has been smoothed to show the shape of the bead more easily. The bead size looks different for both sets of data; it looks larger for the width of the bead than the depth.

3.5.3 Analysis of Depth Mapping Results

Figure 3.25 shows the intensity of a peak from the polystyrene backbone (1001 cm^{-1}) and the v_{CN} intensity (2232 cm^{-1}) on the same plot, from this it is clear that the signal from the tag appears at the same time as the signal from the polystyrene bead. As the polymer stretch is much more intense than the v_{CN}, the intensities have been plot on separate y-axes so that this overlap can be seen.

From the above plots it is possible to see a difference between the depth plot of a dry bead and that of a swollen bead. Both experiments were set up so the bead went from outside the bead on the top side, through the bead and out of the bead on

the bottom side. It is clear to see the shape of the bead from each plot but this is where the difference lies, the swollen bead shows a symmetrical curve about x = 10 which is the middle of the bead, whereas the dry bead shows asymmetric curve around the point x = 0. From these plots it is also possible to fairly accurately estimate the size of the bead, if you assume that where the intensity starts to increase is the top of the bead and that the reverse is true for the bottom of the bead then the size can be calculated. Therefore for the swollen bead this is about 111 μm and for the swollen bead 167 μm. These values can then be compared with white light image of the bead, and hence the width of the bead.

Table 3.7 Table to show the dimensions of the bead in different plots.

Bead Type	Width from White Light / μm	Depth from plots / μm
Dry	68	111
Swollen	158	167

The data highlights the difference in size between the dry and swollen bead, from this table it is clear that the swollen bead is almost double the size of a dry bead. Swelling represents an attempt by the polymer chains to dissolve. The solvents which swell the beads best are those that would dissolve the corresponding linear polymers.[25]

From the above table you can see that the swollen bead shows a consistent size in the width and depth from the comparison of the whitelight and data. The dry bead does not show the same consistency, there is a foreshortening factor of 111/68, which is 1.6. This may be due to the refraction effects, which are explained more in chapter 4.

3.6   Area Mapping

The area mapping of a bead is an extension of the line mapping; it was shown from the line mapping results that there was an even distribution of the 4-cyanobenz-amide across the bead. The use of the area mapping was to hopefully confirm this and to look for features that may not have shown up on the line maps. We started by taking only a quarter of the bead to save time and to perfect the method. Only whole beads are shown in this report though as they give the most information.
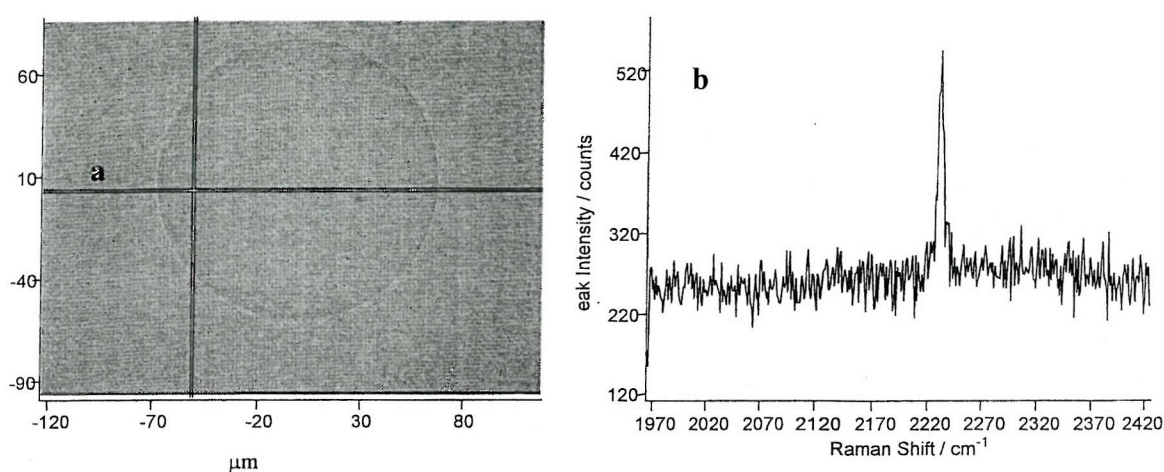
Figure 3.29   An illustration of the mapping software.

The mapping area is drawn on the screen, after the mapping has finished you are able to click anywhere inside the box and the crosshairs (a) will pinpoint the particular spectrum (b) from that point.

The following pages show the area mappings for dry and swollen beads, each map is arranged so that it is possible to see the cross-section through the bead at the same time. Below each set of graphs in have included a picture of the bead in the correct dimensions. It is easier to show the map in the rectangular format when comparing it with the cross-sections but in fact the bead is circular so this representation is shown below the maps in all cases.

3.6.1 Dry Beads
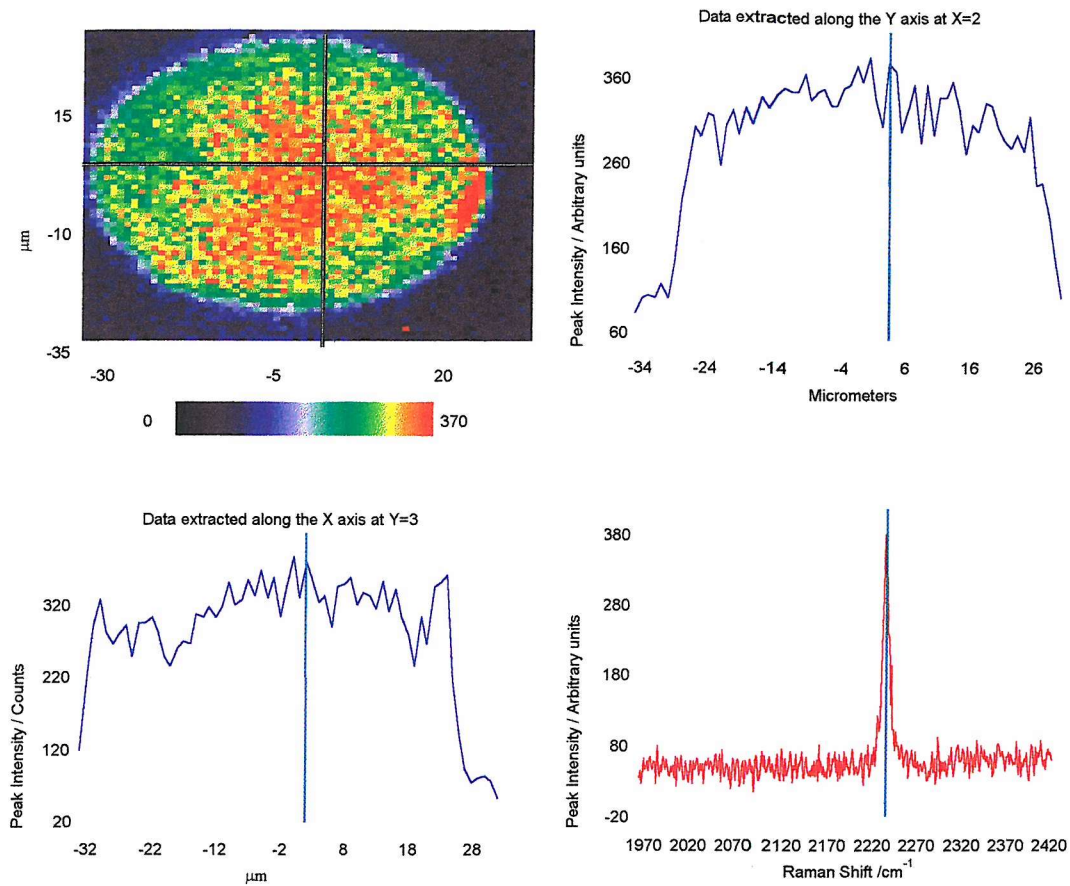
Figure 3.30 Mapping results from a 94 % loaded dry bead. Top left: Bitmap image, Top Right: y-axis cross-section, Bottom left: x-axis cross-section. Bottom right: Spectrum at crosshairs intersection.
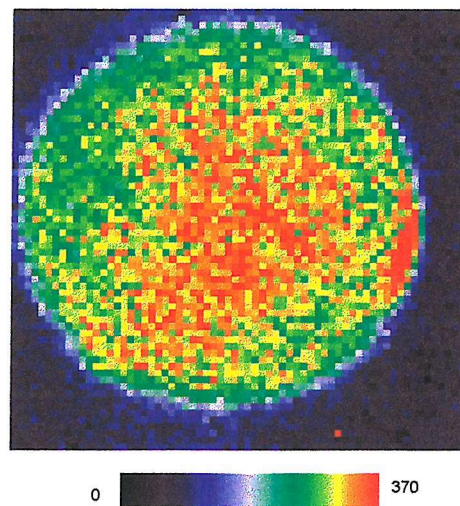
Figure 3.31 True representation of the dry bead.
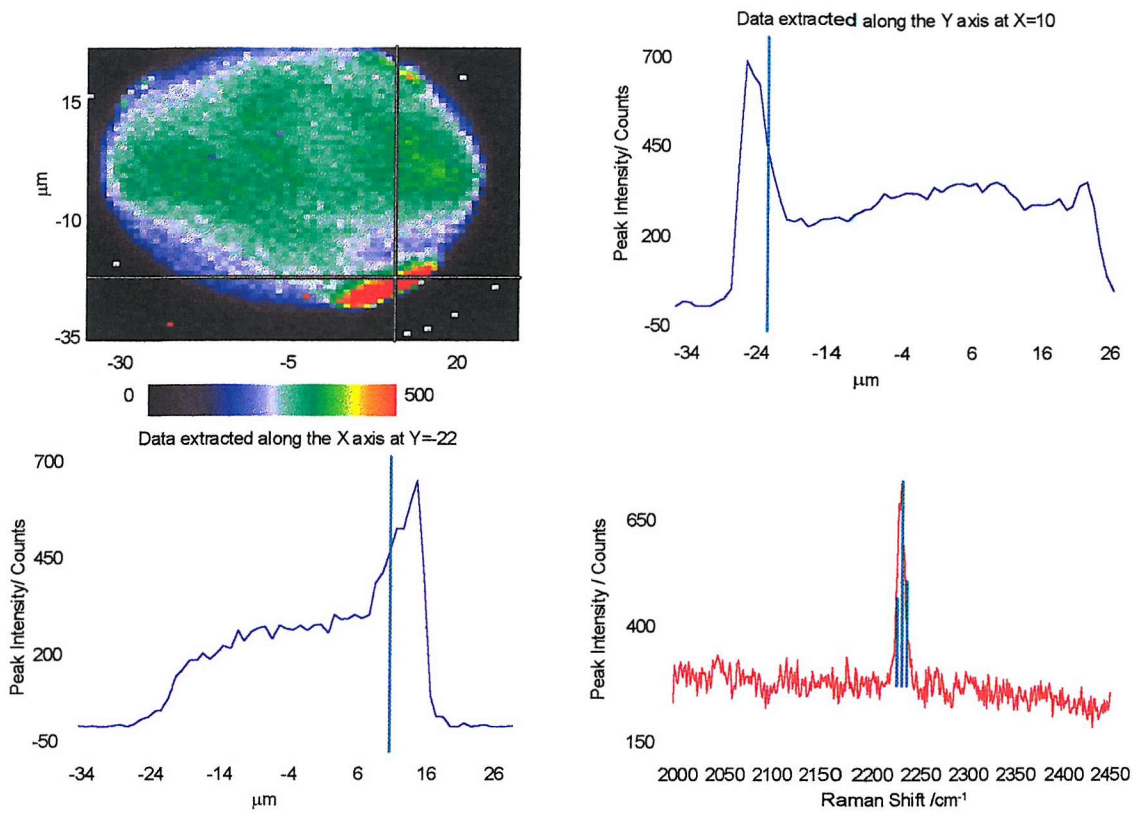
Figure 3.32 Mapping results from a 94 % loaded dry bead. Top left: Bitmap image, Top Right: y-axis cross-section, Bottom left: x-axis cross-section. Bottom right: Spectrum at crosshairs intersection.
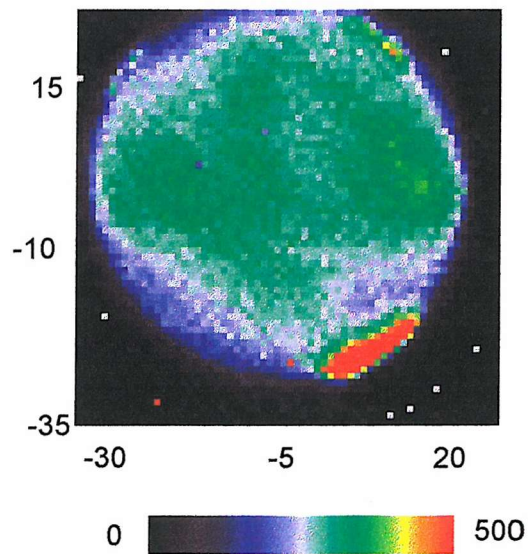
Figure 3.33   True representation of the bead above.

3.6.2 Swollen beads
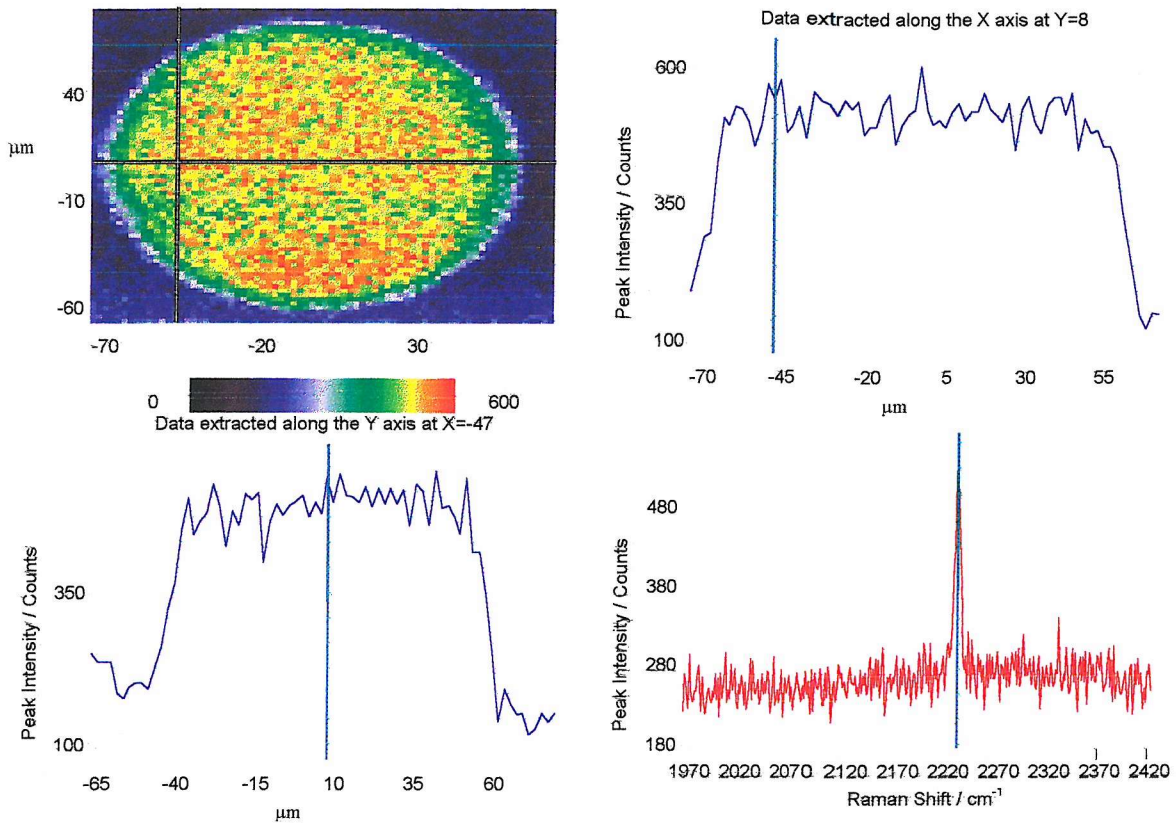
Figure 3.34 Mapping results from a 100 % loaded swollen bead. Top left: Bitmap Image, Top Right: y-axis cross section, Bottom Left: x-axis cross section, Bottom Right: Spectrum at intersection of crosshairs.
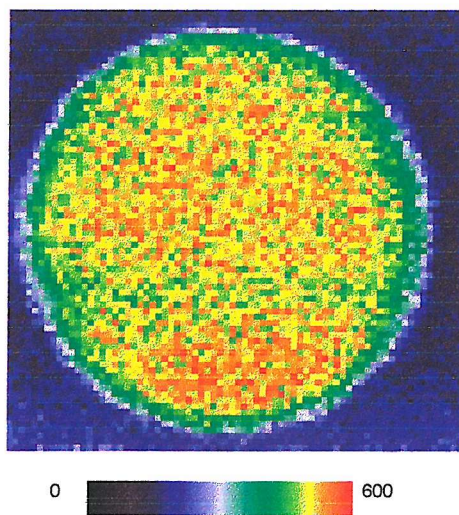
Figure 3.35 True representation of the bead above.

3.6.3   Analysis of area mapping results

Starting with the dry bead (section 3.6.1) it is possible to see how the intensity of the v_{CN} changed across the bead. In Figure 3.30 the peak is most intense in a large area in the middle of the bead and a small area on the right-hand side of the bead. The dark area around the bead shows that no peak at 2231 cm^{-1} is observed, the spectra of the outside of the bead just show noise. The red areas of the bitmap show that the intensity of the peak is at about 370, the green areas show an intensity of about 270, if we take into account the error on the peak intensity (estimated to be 15 %) then this difference in peak intensity is significant. The small intense area of the left is about 12.5 μm^2 in size. Several beads were observed to be not always smooth and have small outcrops of polymer attached. This may be what this feature is, it is interesting though that the cyanobenzamide has intense peaks in this area.

In Figure 3.32 another example of a dry bead is shown. This bead is taken from the same sample of beads but is another taken at random. It shows again an intense area of cyanobenzamide on the bottom part of the bead mapping. This area however is much more intense than the area seen in the dry bead shown in figures 3.30 and 3.31. From the cross sections shown next to the map it is easy to see that the red area has an intensity of ~700, whereas the rest of the bead has an average intensity of about 300. This bead has an edge, which has an intensity of about 150, this however is not an even size around the edge of the bead, and is larger at the bottom of the mapping than the sides. It is however possible to still see the circular shape of the bead, so this uneven edge is not due to the bead being non-circular. Otherwise the bead has an even distribution of v_{CN}, the most part of the bead having an intensity of 360.

The swollen bead (section 3.6.2) shows a more even distribution of the cyanobenzamide with no specific areas where the levels are higher as seen in the dry bead. There is however a band about 9 μm wide around the circumference of the bead which is green. The axis of colour for the swollen bead is larger than in the dry bead so the red pixels represent an intensity of around 600 and the green

represents a peak intensity of around 396. This shows that there is a significant difference between the red and green areas of the map. The slices through the bead shown on the top right and bottom left reinforce what was found in the line mapping that a line drawn through the bead shows an even distribution of the tag throughout the bead. The two line maps also show clearly the edge of the bead, the signal from the ν_{CN} falls away within almost vertically when mapping comes to the edge of the bead.

3.6.3 Peak centre maps

As discovered previously (section 3.2) a relationship was discovered between the loading and the peak centre, I therefore mapped out the distribution of the peak centre on the beads.

- **Dry bead**

2236.2   2238.3 cm^{-1}
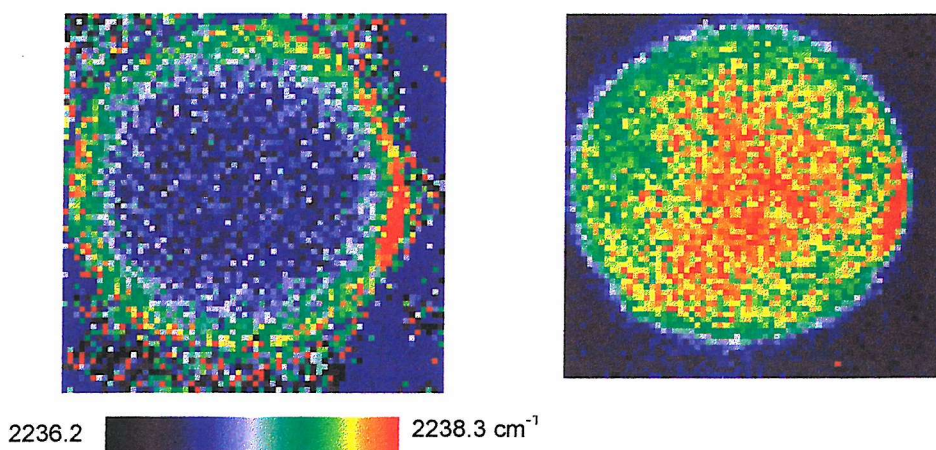
Figure 3.36   **Map of peak centre (left) on a 94 % loaded dry bead and peak intensity (right) for comparison.**

This figure shows a band around the circumference of the bead that has its peak centre at higher wavenumbers than the middle of the bead. There is an intense area of red pixels on the right-hand side of the bead, which shows that it has its peak centre at 2238.3 cm^{-1}, this area corresponds to the same area on the peak intensity map. The range of wavenumbers on this map are not in line with any of the other samples studied, I believe that the calibration of this data is suspect and the

56

wavenumbers should be looked at relative to each other, as the range of 2 cm^{-1} is as expected, and comparable to that of the swollen bead below.
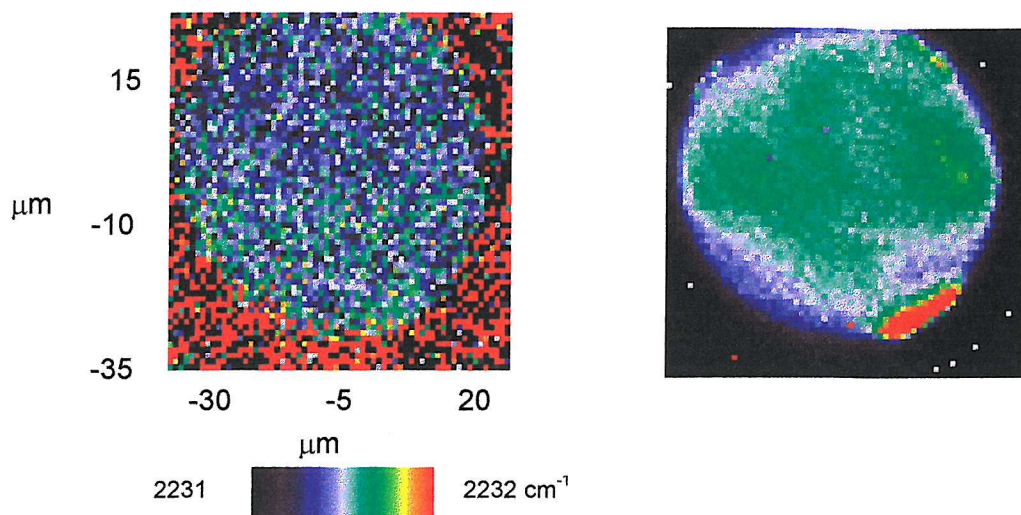
Figure 3.37   Map of peak centre (left) on a 94% dry bead and peak intensity (right) for comparison.

This bead shows a random distribution of peak intensities across the bead. The area of intense ν_{CN} that is seen in the peak intensity maps is not mirrored here in the peak centre mapping. This map as opposed to the other of the dry bead above shows the expected range of wavenumbers for the peak, between 2231 and 2232 cm^{-1}.

- **Swollen bead**
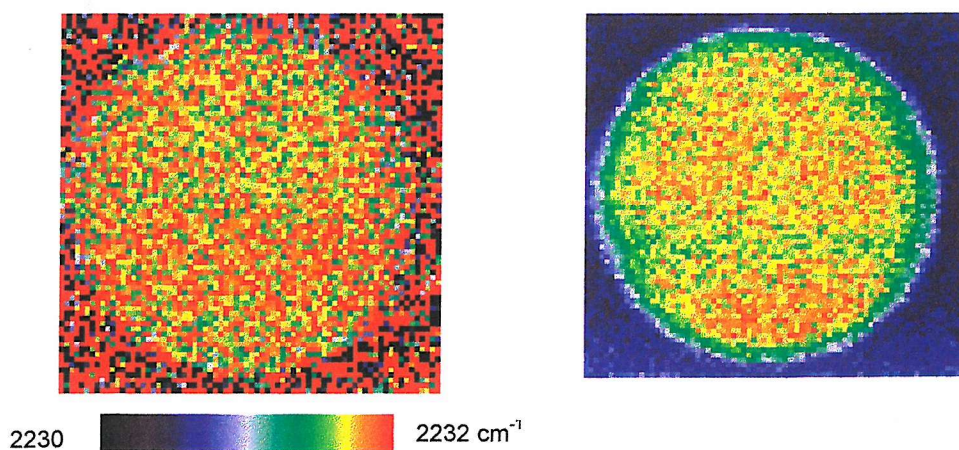
Figure 3.38   Map of peak centre (left) on a swollen bead and peak intensity for comparison (right).

This bead shows a random distribution of peak heights throughout the bead. It is possible to see where the edge of the bead is but there are no clear features on this bead as there are on the dry bead above. Comparison with the peak intensity map shows that the band that is evident around the peak intensity map is not on the peak centre map.

3.7 Atomic Force Microscopy

After mapping the inside of the bead, and noticing that the surface of the bead sometimes had additional pieces of polymer adhered to it, I decided to look at the surface of the bead with Atomic Force Microscopy (AFM).
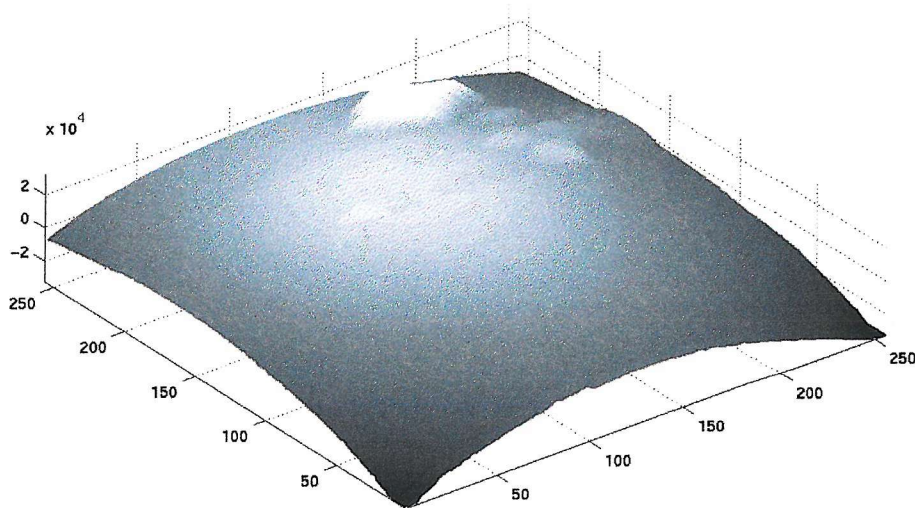
Figure 3.39   Topography results from the bead surface. x-axis: pixels, y-axis: pixels, z-axis: height/arbitrary units.

This result was obtained from a large area of the bead (30 x 30 μm), it shows that the surface is predominately smooth, but that there is an area to the top of these results, which is raised from the surface. This result also shows the curve of the bead.

As this result was done over a large area a smaller area was looked at to see if the surface is as smooth as it looks
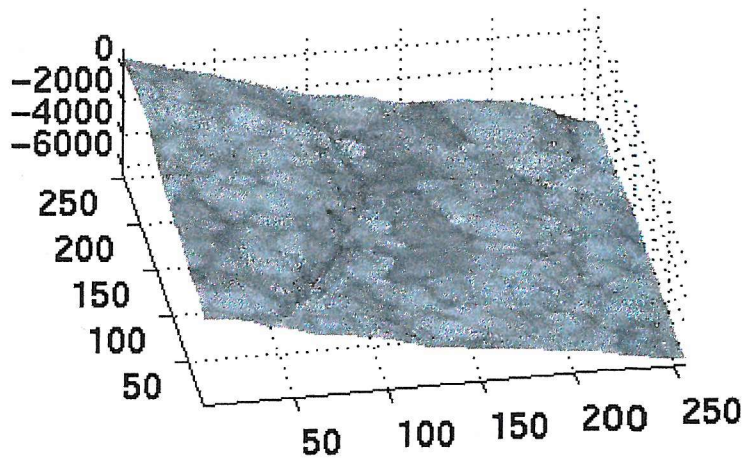
Figure 3.40 **Combined topography and phase results on smaller scale.
x-axis: pixels, y-axis: pixels, z-axis: height/arbitrary units.**

This result shows the surface of a much smaller area of the bead (1 x 1 μm), it shows that the surface is fairly smooth, the colour variation is due to any change in phase and the height change is due to the topography results. There are patches of the bead which cause the change in phase, and also a small ridge can be seen when moving from the left of the figure to the right. The structure seen on this map is about 0.1 μm in size.

4   DISCUSSION

4.1   Raman Spectroscopy of Beads

Raman Spectra were obtained from three types of resin bead. The quality of the spectra was highest for the aminomethylated polystyrene. The nitrile peak (v_{CN}) from the loaded beads was best resolved on the aminomethylated polystyrene beads. This is because Tentagel has a lower loading capacity (typically <0.5 mmol/g) than aminomethylated polystyrene (typically >0.5 mmol/g). As identical experimental conditions were used for both beads, when an identical portion of the bead was analysed less of the cyanobenzamide would have been seen in the Tentagel bead. Therefore polystyrene was chosen as the polymer to be used throughout the rest of the experiments.

4.2   Loading Experiments

4.2.1   Calculated Loading vs. Peak Intensity

In Figure 3.9 a non-linear relationship was observed between the peak intensity and loading for dry beads. There appear to be two trends to this plot, the lower loaded beads (29 –78 %) and the higher loaded beads (85 - 94 %) have an almost linear relationship between themselves. The 73 % and 87 % loaded beads do not seem to fit the trend of either set and either the spectrometer or the ninhydrin test may have poorly measured these beads.
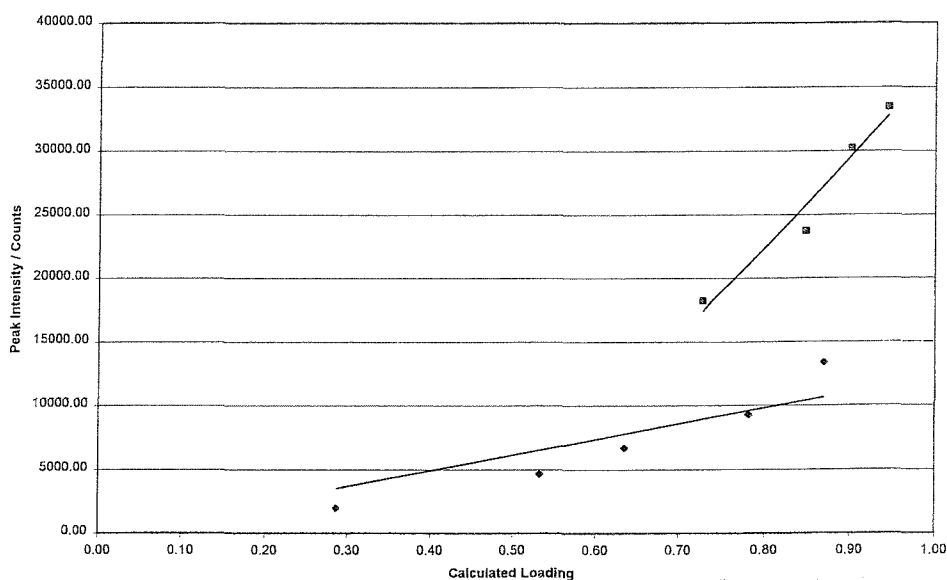
Figure 4.1 Graph to show the two trends in the data.

The intensity versus loading plot for the swollen beads all beads conform well to the curve. The fact that the swollen bead measurements fit a curve better than the dry beads may be due to the uniform nature of the support, in the dry bead there may be areas of higher density of tag. This may be due to the method of drying the beads, they are expanded and shrunk and therefore areas of higher density polymer may form in the dry bead. The measurements were taken non-confocally so a large section of the bead would have been averaged in this scan, which should have decreased this problem, but maybe not entirely eliminated it. A smaller proportion of the bead was observed in the swollen beads as the beads are much larger. The swollen bead has a much more uniform structure due to the presence of the solvent, which may explain the more consistent results.
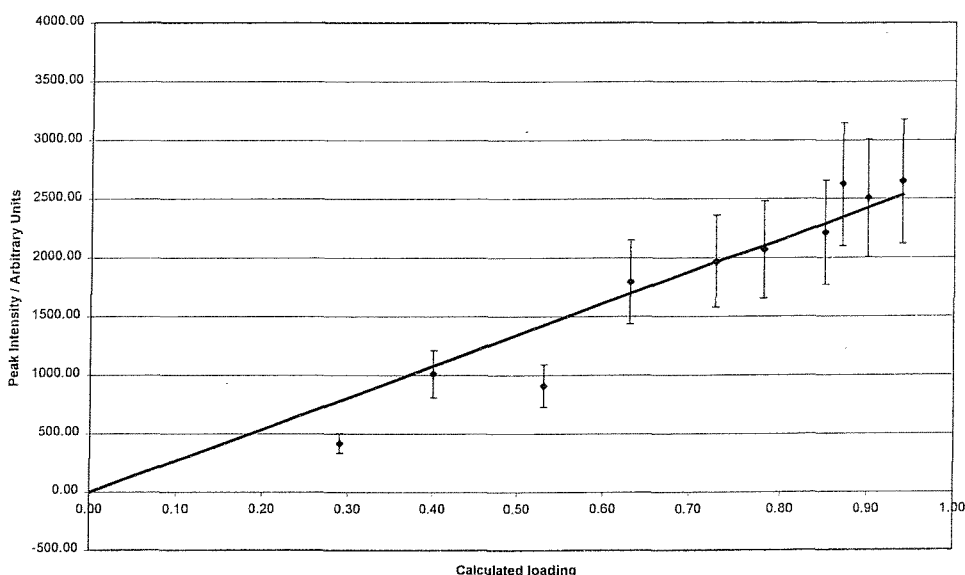
Figure 4.2 Graph to show the peak intensity against the calculated loading for swollen beads. Error bars 20 %.

If the graph is plotted again with the error discovered in the bead distribution section (section 3.3), which is on average 20 % then we see that the data fits well to a linear distribution. The R^2 value for this fit is 0.91, which is a good fit, the trendline also intercepts the y-axis at 0 which is expected, as when there is no cyanobenzoic acid loaded onto the bead there should be no v_{CN}.

4.2.2 Calculated Loading vs. Peak Centre

Figure 3.10 shows that at higher loading in the bead the peak centre of ν_{CN} moves to a higher wavenumber, a shift of 2.5 cm^{-1} is observed. In a dry bead one expects the molecules to be in closer contact, due to the smaller volume of the dry bead, with little chance of movement except twisting around the bond attached to the polymer backbone. In a swollen bead the polymer backbone will be able to move more freely taking the attached molecules with it.

In his paper P. Hodge[25] presents two examples where reactions occurred between different molecules bound to the same resin bead. This implies that there are considerable interactions between a large percentage of molecules bound to the resin. In a linear polymer it is conceivable that in time all sites will encounter each other. The cross-linking in the polymer bead will limit this mobility but it will not be extensive enough in a 1 % cross-linked resin bead to isolate any of the sites extensively. In one of these experiments, residues supported by the same polymer came together reacted and then separated, No new cross-links were formed. It was found that as the percentage cross linking increased from 2 to 37 % the minimum number of sites reacting decreased from 47 to 0 % respectively.

When loading with 4-cyanobenzoic acid as more and more is added the distance between these molecules becomes smaller and so they interact to a greater extent with each other. The distance between the tag molecules can be calculated, as we know the size of the beads and the number of sites on the bead. The calculation assumes a volume around the tag. It is the distance between these volumes that is calculated. The equations and working are shown in the Appendix and the results are shown below.

Table 4.1 Table to show the separation of tags in a beads with different diameters.

Diameter of Bead / μm	Loading Fraction	Separation / nm
200	1	3.9
150	1	2.9
100	1	2.0
50	1	1.0

Table 4.2 Table to show the separation of tags in a bead with different loadings.

Diameter of Bead / μm	Loading Fraction	Separation / nm
100	1.0	2.0
100	0.75	2.6
100	0.5	3.9
100	0.25	7.8
100	0.1	19.6

The results in the above tables show that when the loading is very high the tags are extremely close together. Therefore the chance of interactions between the sites is very high.

There are many interactions that can occur between the molecules, these include dipole-dipole interactions, dipole-induced dipole interactions, induced dipole-induced dipole interactions, and hydrogen bonding.
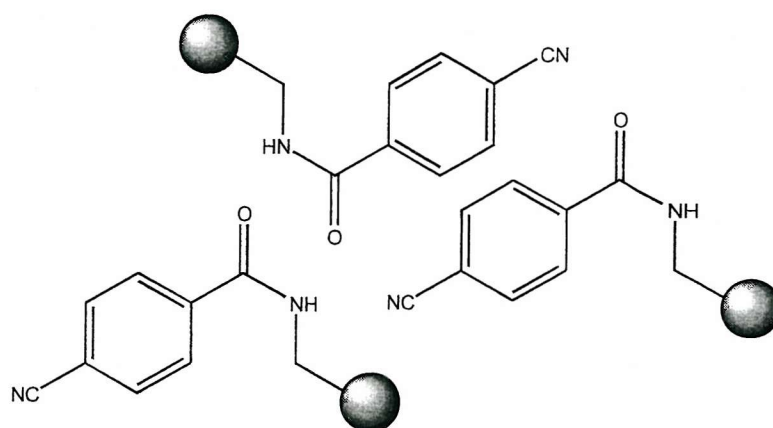
Figure 4.3   Diagram to illustrate the interactions in the loaded bead.

Hydrogen bonding will occur between the double bonded oxygen of the amide bond of one molecule and the hydrogen attached to the nitrogen on another molecule. This will be an attractive force between the two molecules. Hydrogen bonds will be set up throughout the resin forming a network of attracted molecules. A negative interaction will take place between the π systems of the conjugated ring

64

structure. The π system above and below the ring is negative in nature therefore the rings will repel each other. Dipole interactions will occur between the electronegative oxygen and electropositive nitrogen, these will be weak interactions but positive in nature.

These interactions between molecules produce the shift in the vibrational frequency of the nitrile stretch. Erik J. Hutchinson and Dor Ben-Amotz [26] found that the frequency of the vibration shifted with an increased density of molecules. Using 1-octene they looked at the C=C bond density dependence of the frequency shift and force over a gas to high pressure density range. They used IR and Raman spectroscopy to measure the forces between molecules as the change in force can be measured directly by these forms of vibrational spectroscopy. They found a frequency shift of 8 cm^{-1} when increasing the pressure from 4 to 5.2 molecules nm^{-3}.

4.3   Bead Distribution

4.3.1   Peak Intensity

The histograms and statistical data presented in section 3.3.1 show the spread in intensities across a sample of 20 beads for 3 differently loaded samples. The 29 % and 94% loaded beads fit well to a Gaussian curve but the 73 % loaded sample fits badly. The 73 % sample set does not indicate that choosing a bead at random would represent the whole of the set, but if you look at Figure 3.9 then you could say that this data point does not fit the trend of the curve. Therefore that sample of beads may be faulty in some way and all the beads may not have reacted or not have been quenched in the correct way. This may also be due to the small sample set used, a larger sample represents the population better and gives a clearer indication of the sample's properties.

4.3.2   Peak Centre Position

The histograms for the peak centre position do not fit a Gaussian curve very well the 73 % (Figure 3.18) and 94 % (Figure 3.19) loading samples show better fits to the Gaussian but the 29 % (Figure 3.17) sample shows a very poor fit. Although if you look at the scale on the bottom of the graphs you can see that on average they span only 0.8 cm^{-1}. The spectral resolution of the spectrometer is about 0.1 cm^{-1};

however the accuracy to which the silicon was calibrated was about 1 cm^{-1}, therefore all the sampled beads are within this error. If you look at the statistical data presented in Table 3.6 then a trend is seen in the shifting of the peak centre with loading. At 94 % loaded the peak centre is at higher wavenumbers than the 29 % loaded bead, this is the same trend as seen in the loading experiments as discussed in section 4.2.2.

4.4 Line Mapping

The line mapping results showed that the dry beads had a constant level of cyanobenzamide across the bead. This result was to be expected if the reaction of the 4-cyanobenzic acid with the aminomethylated functionality of the bead is not diffusion controlled. If the reaction were diffusion controlled it would be expected that the lower loaded beads would show an increased intensity of the nitrile stretch on the edge of the bead where the reactions would take place initially. All the beads were in the same reaction vessel but at different times a small quantity of beads were removed and the coupling reaction quenched, hence the reactant molecules would not have been able to permeate to the middle of the bead if there was a diffusion problem. If the differently loaded beads had been generated in a way where an increased amount of the reactant was used in order to produce increased loading, then all the beads would have had a diffusion edge on them where the reactant had reacted as far as it had diffused. Diffusion will be faster at higher concentration as there will be a larger concentration gradient.

As the reaction is not diffusion controlled, it is clear that the beads, which are swollen when the reactions occur, are no longer solid in nature but like a gel as there is no steric hindrance to limit the reactants path to all the functional groups within the bead. The beads swell extremely quickly. This was observed while performing the reactions on swollen beads. After placing the bead in the dioxane the beads expanded to about double their size starting from the edge and moving towards a core of unswollen bead until it was all in a swollen state, this takes about 10-15 seconds.

The dry beads show a constant level of cyanobenzamide through the bead but the swollen beads show a decrease in the v_{CN} intensity towards the edge of the bead. This same decrease is seen in the swollen beads on the area mapping so I will discuss it further in section 4.6.2.

From all the line mapping graphs it is easy to see that at better resolution more data points are seen across the graph hence showing the structure that is present at the 1 μm level. Therefore in the area mapping data was collected every one or two microns in the x and y direction.

4.5 Depth Mapping

The depth mapping measurements show a difference between dry and swollen beads. This difference is seen in mapping through the bead, the main differences between the dry and swollen beads are the difference in the shape of the map and the comparison with the white light image.

The difference is due to the lensing effect of the bead. Yan and Kumaravel [27] describe in the literature how they use a flattened bead as it improves the quality of the spectra in Infrared spectroscopy. They do not provide much explanation why but comment that 'one cause for this (decreased interference from flattened beads) is probably the long and irregular pathlength the incident beam has to pass through a globular bead' they flatten the bead to give a sample with a short and uniform pathlength.

The dry bead and swollen bead are different when measured due to the environment around them. The dry bead is surrounded by air, hence there is an air /polystyrene boundary, whereas the swollen bead is so swollen that the environment is almost totally that of the solvent, a solvent/solvent boundary is formed. This difference has an effect on the propagation and scattering of the light going into the bead. The boundary of the dry bead changes the angle of the light as it enters the bead. This is due to a depth illusion effect as seen when looking into clear pools of water. The bottom always looks closer than it is due to focusing.

This effect occurs at the flat boundary of the air/solvent and would also occur at a flat bead/air boundary. The curved interface of the bead gives additional effects.
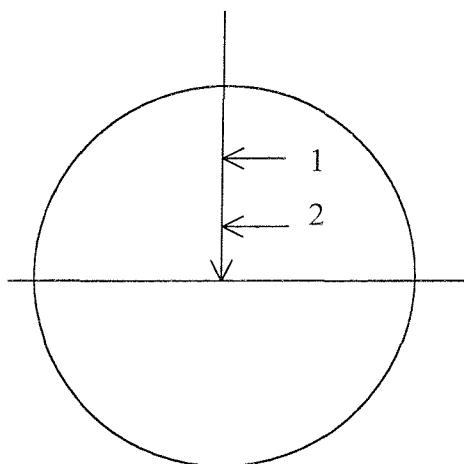
Figure 4.4   **Depth focusing of a bead. Position 2 is where one thinks they are focused and position 1 is where they are actually focused.**

This effect of the focus being higher than expected is dependant on the angle of incidence of the light on the bead, at higher angles the beam is refracted more towards the middle of the bead and the actual position is lower than the apparent position. This is because of the angle of incidence and refraction (Snell's law).

$$n_{air} \, sin\theta_1 = n_{poly} \, sin\theta_2$$

Where **n** is the refractive index of the material and θ_1 is the angle of incidence and θ_2 is the angle of refraction. As θ_1 increases, θ_2 decreases, hence the beam is refracted towards the middle of the bead.

With respect to the depth map of the bead this effect creates problems with mapping through the bead in confocal mode, the laser light is refracted through the dry bead hence an unsymmetrical distribution is seen through the dry bead on the depth mapping. This may explain why the whitelight image and the mapping do not agree in size. The whitelight image was almost half the size of the mapping

68

result, this may be a result of the actual and apparent focus but this difference seems much larger than this effect so may be described by another effect.

The swollen bead however does not have the same problems, this is because the same boundaries do not exist because the solvent has totally swollen the bead and the bead is mostly solvent. The difference in the index of refraction between dioxane and polystyrene is very small (polystyrene, 1.59, dioxane, 1.42 and air 1.00). Even before swelling the refraction of the light would be much smaller than an air/polystyrene boundary, once swollen the effective refractive index of the bead will be that of the solvent and hence the apparent focus and actual focus will be closer. This may be why the depth map of the swollen bead is symmetrical and the white light image and the map compare favourably in size.

The depth mappings presented in Figure 3.28 show the depth and width measurements of a swollen bead overlaid. The smoothed lines on them show up the slight difference in the size of the bead when measured in the z-direction or in the x-y plane. If these two sets of data are separated and a box drawn around the data as shown in Figure 4.5 with the sides of the box starting at the side of the bead then an estimate of the size of the bead can be obtained.
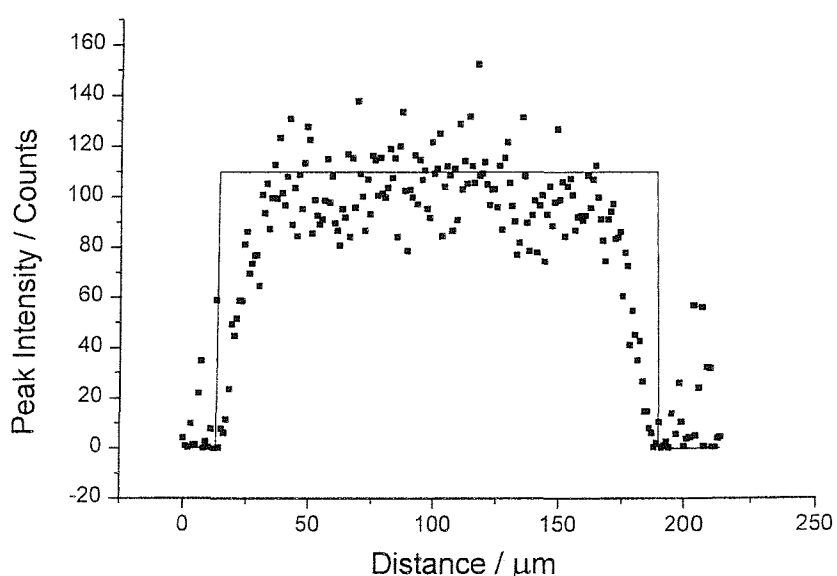
Figure 4.5   Width measurement of swollen bead with analysis box drawn.

The vertical sides of the box are drawn as soon as the intensity starts to increase from the baseline level. The horizontal line is drawn through the average points and again the vertical line is drawn where the edge of the bead is believed to be. This operation was performed for both sets of data in Figure 3.28 and the results are shown below.

Table 4.3   Results of depth and width measurements of a swollen bead.

Measurement	Length of bead / μm
Width	175
Depth	168

These results show that when the bead is swollen that it has eliminated most of the problems with refraction, as the bead appears the same length in both the depth and width measurements. However if you look at the results obtained from the dry bead as outlined in Table 3.7 then the difference in the results is larger. The foreshortening factor is 1.6 this is the same ratio as the refractive indices of polystyrene and air, the two different materials used in this experiment.

To rectify the problems with the dry bead, a solvent with a similar refractive index to the polystyrene could be used so as to minimise the refraction problems. A sugar solution could be made as the higher the concentration of sugar the higher the refractive index. This solution would still keep the beads dry, as water does not swell the bead so they would just be surrounded by the sugar solution.

4.6   Area Mapping

4.6.1   Dry Beads
These results showed how the bead could be mapped using confocal Raman spectroscopy. The line mapping showed how the levels of cyanobenzoic acid changed across the bead but it was not possible to show up any small areas that would have shown a deviation in the signal when line mapping.

The advantages of the area map show up immediately with the mapping of the dry bead; the results show a small area on the right hand side of the bead that has a

more intense signal for the ν_{CN}. This area would not have shown up to the same degree in a line mapping it would just have shown an increase in the signal in that section of the bead which would have been put down to the fluctuations in the signal across the bead. These results from the mapping of the dry bead may not actually represent the whole of the bead as expected due to the lens problem.

The bead is acting as a lens and refracts the beam of light towards the middle of the bead as shown in the figure below.

——————— Path of light

.... Expected Path of Light
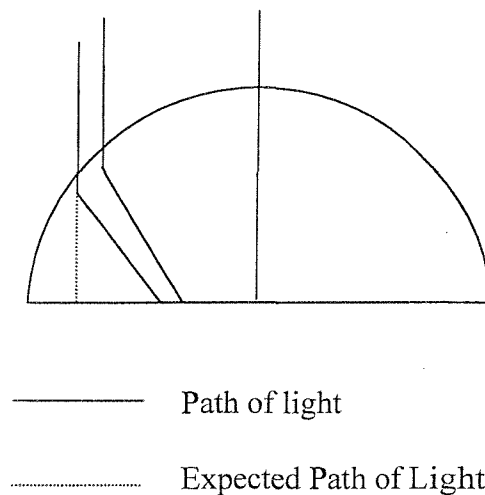
Figure 4.6   Diagram to show the light path in a dry bead when area mapped.

The figure shows that when we were mapping through the dry bead and thought we were mapping the area we were looking at directly with the white light, that in fact the light was being diffracted and was mapping an area towards the centre of the bead. Only exactly in the middle of the dry bead is the light behaving in the way we expect. Therefore the data represented in the maps is skewed somewhat, but as we now know how the data can be unscrambled. The map does not need to be disregarded as it still provides information about the inside of the bead but it does need to be noted that the scaling of this information is not as represented in the map. From the light path in Figure 4.6 it is clear to see that the data in the map comes mostly from the centre of the bead, even the light which illuminates near to the edge of the bead is shown back towards the middle.

The other problem which needs to be investigated is the apparent and actual focus position as highlighted in section 4.5 p 67. When we set up the bead for mapping we were confident that the mapping was to take place in the centre plane of the bead by using the white light to focus onto that area. As the bead is acting like a lens and the apparent focus is different to the actual focus, it is conceivable that we did not take a flat slice through the exact middle but probably a curved surface slightly above the middle, as illustrated below.
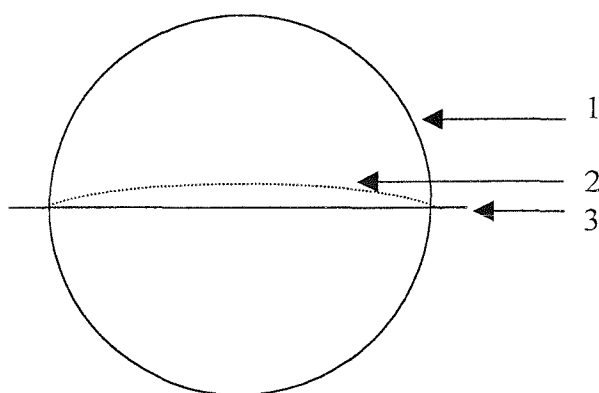
Figure 4.7   Area mapping surface. Key: 1 Bead, 2 Actual surface mapped, 3 Assumed surface mapped.

This does not have any real effect of the map; it should just be noted that the slice taken is not flat but a slight curve. It is the refraction of the light through the bead that is the most significant problem for a dry bead.

If we therefore look again at the results again but noting that the scale may not be accurate we still see areas on the bead that have a higher v_{CN} intensity than other areas, this difference is significant. The small area on the right of the map(in Figure 3.30 and Figure 3.32) is assumed to be a small outcrop of polymer (this was also noticed visually on some beads). This area was not noticeable on the white light image of the bead, but this may be due to the focus, if it was underneath the bead slightly, the top of the bead would have obscured it. If this area was a drop of polymer that became attached to the bead after the initial forming of the bead there may be a boundary between this area and the rest of the bead. If this were true then the reactant would have diffused into this area during the reaction step and not been

able to process further into the bead, therefore forming an area of increased concentration of cyanobenzoic acid and hence a stronger v_{CN} intensity.

In Figure 3.30 (the first dry bead) the other area of higher intensity is towards the middle of the bead, although this is not as pronounced as the small area. The middle of the bead shows some variation in the intensity of the peak but is mostly of higher intensity when compared to the edge of the bead. This localisation of intensity may be caused by the refraction problem, as commented above, the map was taken from a predominate part of the centre of the bead. Therefore this high intensity may have arisen from a small section of the centre of the bead and not be a widespread as the map indicates. There is then the question of why the intensity of the peak is significantly higher in the centre. This can not be explained by the sampling volume as when the instrument is sampling in confocal mode the edge is only three μm deep, as soon as you move three microns into the bead the volume sampled is full of bead. The area around the edge of lower intensity is much larger than this.

Figure 3.32 shows a more consistent intensity of v_{CN} through the bead, however this may be due to the extended scale, which is needed for the very intense area of the bead. The average peak intensity across the bead is ~300 counts, if the colour scale had been shorter then variances in this area may have shown up more clearly. The interesting feature, which is seen on this bead though, is the uneven edge. There is an area at the bottom of the mapping, which shows a much wider area of lower intensity, which is attributed to the edge of the bead. As above this is much larger than the edge of the bead, and must be due to a non-uniform distribution of the cyanobenzamide.

Mapping of beads in this way has not been carried out before so there are no results to compare ours with. Haap and co-workers [28] used FT-IR to map whole samples of beads to distinguish between different beads that had been generated through mix and split. The beads were embedded in a KBr window and a 3 mm by 3 mm scan carried out, by mapping for different vibrations each time a distinct sample of the set showed up. It was possible to overlay the maps with the white light image of

the beads to discover which bead contained which functionality. The advantage of this over mass spectrometry was that it could be carried out without destruction of the sample and with spatial resolution. This method did not necessitate the need for tags as the compounds themselves were tags and the beads could be pinpointed by the map overlays.

The literature has stated that 99 % of the functional groups will be inside the bead [25,29]. This was proposed from volume calculations. By knowing the quantity of reactive groups from the bead from measurements such as the ninhydrin test and the number of sites on the surface it was possible to deduce that the rest of the sites were inside the bead. This was only a hypothesis until now, we have shown by mapping through the bead with confocal Raman spectroscopy that the reactive sites of the bead are in the interior of the bead, as we have attached a tag to these sites.

4.6.2 Swollen Bead

As outlined above the swollen beads do not have the same problem with refraction as the dry beads. This is due to the minimal boundary between the polystyrene and dioxane. Therefore the maps obtained for the swollen beads are a truer representation of the bead and do not need correcting, as the light was not refracted towards the middle. The problem that does still exist but not to the same degree is the actual and apparent focus problem. The swollen beads also have a curved slice taken through the middle rather than a flat plane as expected.

The area map of the swollen bead shows a bead with a distribution of intensities in the middle and an edge of lower intensity. This decrease in intensity was also seen for the line maps of the swollen beads. As I have commented before, this is not due to a lower density of polymer in the sampling volume as we move towards the edge because the instrument uses the confocal volume, which is constant throughout the bead.

If we look at the cut through segments of the bead that are presented with the maps we can see that the edge of the bead is quite sharp, this is the same area that has the lower intensity and is only over about 4 μm/pixels. I believe that the volume of the

bead being measured at this point is much smaller than the edge, but I think it is the edge that is causing the decrease in intensity, as the swollen bead has on whole a even distribution of tag throughout it. If we look again at the slices taken through the bead and drew lines of best fit through the data we would in fact draw a box, the edges would become straight and the variance in the intensity on the top would also have a straight line drawn through it. The bitmap image helps to put these pieces together but can also distort them.

4.6.3 Peak Centre Maps

The dry bead peak centre map shows areas of different peak centre. In Figure 3.36 a band around the outside indicates higher wavenumbers, this corresponds to some extent to the slight edge around the mapping of peak intensity of the dry bead, again on this measurement we need to be aware of the focusing problems as illustrated in section 4.5. The area that is clear on both maps (peak centre and peak intensity) is the small outcrop on the right hand side of the bead; this shows the most intense peak and the highest wavenumber. If we refer to the loading experiment graphs (section 4.2) then you can see that I observed that at higher loading the peak centre was shifted to higher wavenumbers, therefore this phenomenon is being shown here. I believe this fits with the theory that I put forward earlier that a high concentration of tag is trapped in an outcrop of polymer and therefore gives the signals shown.

Figure 3.37 does not show the same change in peak centre on the high intensity area of the map. The peak centre map shows a much more even distribution of peak centres, the area where the intense region of tag was observed could show a slight increase in peak position but not as pronounced as in the other dry bead (Figure 3.36).

The swollen bead which lacks a lot of the focusing problems shows a very random distribution of wavenumbers for the peak centre across the bead, the edge that is seen in the peak intensity map is not seen at all in the peak position map. This randomness of peak position was seen in some degree in the loading experiments; the plot of peak centre against loading did not show a clear trend towards higher

wavenumbers. It should be noted that the problems with refraction do not in anyway change the frequency of v_{CN}, but just where the information came from.

The dry bead in Figure 3.36 shows a problem with the calibration of the peak centre, the instrument is calibrated everyday with silicon as this has an intense peak at 520 cm^{-1}. The spectrum is taken of the silicon and the peak centre adjusted to this number within 0.5 cm^{-1}. Other spectra taken on the same day were examined and these are correct. It is believable that the calibration went amiss before this experiment started and therefore the peak centres for this data should be taken as arbitrary. In the future the silicon calibration should be done more accurately so that from day to day the data can be compared with more ease. For example if you compare the data in the loading experiments (section 3.2.1 p 39) with that of the bead distribution (section 3.3.3 p 41) then you can see a difference. The data varies by about one wavenumber, but both show a trend towards higher wavenumbers for higher loading.

4.7 Atomic Force Microscopy

These experiments were performed to reinforce the case for the lens effect; it was thought that if the bead showed a smooth surface then it would act more like a lens. If a surface is uneven and irregular then the light is not scattered in a uniform way and the prediction of where the light was refracting through the bead would have been more difficult. The results shown in section 3.7 show that the surface on the whole is smooth, the scan performed over the larger area shows a bump in the top corner, this confirms the presence of irregularities on the bead which had been noticed through the microscope and is also present on the dry bead area mapping (section 4.6.1). The results from the smaller area show that there is some structure at about 0.1 μm this shows up when the topography and phase data are combined. This roughness is so small that the bead still acts like lens. A small step is seen on the bead this maybe part of a larger defect on the surface, although the step does not have edge, it slopes onto the rest of the area.

These results therefore confirm the presence of a lens effect in the beads. The surface is smooth and would refract the light evenly over the surface, this refraction

would be disturbed if a bump was found on the surface, but these are quite small and not seen on every bead, although they may be more common than previously thought.

5 CONCLUSIONS

The aim of this project was to use confocal Raman spectroscopy to look at the nature of the resin beads and the distribution and properties of tags once loaded onto the beads.

It has been shown that the loading of a Raman active tag onto the active sites of a bead does not give a linear relationship between the loading and the peak intensity of the CN stretch for a dry bead. This is due to the intermolecular interactions inside the bead as they come closer together when loaded in higher concentrations. The swollen bead shows a more linear relationship between loading and the peak intensity, this is due to the more uniform nature of the support when swollen. As only one bead was used for each experiment I checked that these were a good representation of the sample, the results show that on the whole a bead selected will be characteristic of the sample. To produce results that are truly typical of the sample though, several beads should be measured and the results averaged.

The mapping of the beads helped to understand the distribution of the tag through the bead, the line and depth maps showed that there was an even distribution of the tags through the bead and that the tag and polymer were found together. These maps also showed that the reaction was not diffusion limited, as higher proportions of the tag were not found on the outside perimeter of the bead.

It is thought that the beads probably act as a lens, beads have been flattened in previous experiments performed in the literature to improve the spectral quality but no reason has been given for this, it is not believed that other groups have looked into this problem. The lens effect is a larger problem when measuring dry beads as the light is refracted more, with swollen beads, as the solvent is such a large percentage of the bead, a large part of the lens effect problem disappears. Swollen beads are more representative of the beads used in combinatorial chemistry though as all reactions are carried out in excess solvent when the bead is in a swollen state. The lens effect when quantified and calculated can be compensated for, so that maps can be rectified to give the correct information, this has not been done in this report.

The mapping of whole beads gives more information on the distribution of tags through the bead. They help to show up areas of the bead that wouldn't have been noticed in the line maps, the dry bead for example shows a small outcrop of polymer on the side of the bead, this phenomenon is also seen on with the atomic force microscopy. This is not true for all beads but is a feature of some of them. It would be interesting to perform further area maps but difficulties exist in gathering the information effectively. The dry beads are simpler to map than the swollen beads, but the swollen beads give more relevant information. The problem with the swollen beads is their movement in the solvent. The apparatus we used was sufficient but a more sophisticated set-up may help the bead to be swollen and immobile for the length of the experiment (>15 hours) and eliminate the problem of solvent evaporation. The area maps reinforce the line maps in showing that the tag is distributed evenly through the bead.

6 REFERENCES

(1)   Combinatorial chemistry:winning the chemical lottery. In *Chemistry and Industry*, 1998; Vol. 19; pp 757.

(2)   S. Borman. Combinatorial chemists focus on small molecules, molecular recognition and automation. In *Chemistry and Engineering News*, Feb 12,1996; pp 29.

(3)   G. Bhalay. A lottery for Chemists. In *Chemistry in Britian*, March 1999; pp 25.

(4)   N. K. Terrett *Combinatorial Chemistry*; Oxford University Press: Oxford, 1998.

(5)   J. W. Guiles; C. L. Lanter; R. A. Rivero. *Angewandte Chemie-International Edition* 1998. **37**, 926.

(6)   R. H. Scott; S. Balasubramanian. *Bioorganic & Medicinal Chemistry Letters* 1997. **7**, 1567.

(7)   B. J. Egner; S. Rana; H. Smith; N. Bouloc; J. G. Frey; W. S. Brocklesby; M. Bradley. *Chemical Communications* 1997, 735.

(8)   S. S. Rahman; D. J. Busby; D. C. Lee. *Journal of Organic Chemistry* 1998. **63**, 6196.

(9)   B. D. Larsen; D. H. Christensen; A. Holm; R. Zillmer; O. F. Nielsen. *Journal of the American Chemical Society* 1993. **115**, 6247.

(10)   Q. Sun; B. Yan. *Bioorganic & Medicinal Chemistry Letters* 1998. **8**, 361.

(11)   B. Yan. *Accounts of Chemical Research* 1998. **31**, 621.

(12)   B. Yan; G. Kumaravel; H. Anjaria; A. Y. Wu; R. C. Petter; C. F. Jewell; J. R. Wareing. *Journal of Organic Chemistry* 1995. **60**, 5736.

(13)   B. Yan; H. U. Gremlich. *Journal of Chromatography B* 1999. **725**, 91.

(14)   B. Yan; Q. Sun; J. R. Wareing; C. F. Jewell. *Journal of Organic Chemistry* 1996. **61**, 8765.

(15)   H. U. Gremlich. *Biotechnology and Bioengineering* 1998. **61**, 179.

(16)   B. Yan; H. U. Gremlich; S. Moss; G. M. Coppola; Q. Sun; L. Liu. *Journal of Combinatorial Chemistry* 1999. **1**, 46.

(17)   D. E. Pivonka. *Journal of Combinatorial Chemistry* 2000. **2**, 33.

(18)   R. Gale *Spectroelectrochemistry -Theory and Practice*; Plenum Press: New York, 1988.

(19) P. Hendra; C. Jones; G. Warnes *Fourier Transform Raman Spectroscopy, Instrumentation and Chemical Applications*; Ellis Horwood: Chichester, 1991.

(20) T. Wilson *Confocal Microscopy*; Academic Press: London, 1990.

(21) R. Borlinghaus; B. Grobler. Basic Principles and Applications of Confocal Laser Scanning Microscopy. In *Modern Optics, Electronics and High precision techniques in cell biology.*; Isenberg, G., Ed.; Springer: Berlin London, 1998; pp 34.

(22) D. F. Edwards; E. Ochoa. *Applied Optics* 1980. **19**, 4130.

(23) *CRC Handbook of Chemistry and Physics.*, 58th ed.; CRC Press Inc.: Cleveland, Ohio, 1977.

(24) V. K. Sarin; S. B. H. Kent; J. P. Tam; R. B. Merrifield. *Analytical Biochemistry* 1981. **117**, 147.

(25) P. Hodge. *Chemical Society Reviews* 1997. **26**, 417.

(26) E. J. Hutchinson; D. Ben-Amotz. *Journal of Physical Chemistry B* 1998. **102**, 3354.

(27) B. Yan; G. Kumaravel. *Tetrahedron* 1996. **52**, 843.

(28) W. J. Haap; T. B. Walk; G. Jung. *Angewandte Chemie-International Edition* 1998. **37**, 3311.

(29) B. Yan. *Combinatorial Chemistry & High Throughput Screening* 1998. **1**, 215.

APPENDIX

Calculation of separation between tags on beads.

Volume of Bead $= \dfrac{4}{3} \pi \cdot r^3 = V$

Molecular Separation $= x$, assume uniform distribution within bead.

Number of sites in the bead $= N$

Volume around each molecule $= \dfrac{V}{N}$

Radius of cell around tag $= \dfrac{x}{2}$

Volume of each cell $= \dfrac{4}{3} \pi \left(\dfrac{x}{2}\right)^3 = \dfrac{\pi x^3}{6}$

Therefore the volume of the cell is the same as the volume of the bead divided by the number of sites.

$$\dfrac{\pi x^3}{6} = \dfrac{4}{3} \dfrac{\pi \; r^3}{N}$$

$$x^3 = \dfrac{4}{3} \dfrac{\pi r^3}{N\pi} \times 6$$

$$x^3 = \dfrac{17.5 \times r^3}{N \times \pi} = \dfrac{5.6 \times r^3}{N}$$

$$x = \left(\dfrac{5.6 \times r^3}{N}\right)^{\frac{1}{3}} = \dfrac{1.8r}{N^{\frac{1}{3}}}$$

If r is 50 μm and N is 10^{14} sites bead^{-1}

$$N^{\frac{1}{3}} = \left(100 \times 10^{12}\right)^{\frac{1}{3}} = 4.6 \times 10^4$$

$$x = \dfrac{1.8 \times 50 \times 10^{-6}}{4.6 \times 10^4} = 1.96 \times 10^{-9}\,\text{m}$$